Confined Quantum Molecular Degrees of Freedom

by

Jianying Sheng

A thesis
presented to the University of Waterloo
in fulfillment of the
thesis requirement for the degree of
Master of Science
in
Physics

Waterloo, Ontario, Canada, 2017

I hereby declare that I am the sole author of this thesis. This is a true copy of the thesis, including any required final revisions, as accepted by my examiners.

I understand that my thesis may be made electronically available to the public.

Abstract

Motivated by recent experimental measurements of the degeneracy lifting of the rotational ground state of molecular ortho-H_2 confined inside the fullerene cage C_{60} and, more generally, motivated by the physics of confined quantum molecular degree of freedom. By using exact diagonalization we performed a detailed study on the coupled translational and rotational motion of H_2 based on the Van der Waals interaction model. We found that degeneracy lifting is caused by a symmetry reduction from Ih to C_{3i} symmetry of C_{60} in its solid state. The origin of the degeneracy lifting is found to mainly arise from the interaction between H_2 and its C_{60} cage instead of the interaction between the $H_2@C_{60}$ molecule and its neighbouring molecules. The size of the splitting is extremely sensitive to the cage geometry while sitting in a relatively large linear regime. The zero point motion effect of carbon atoms does not change the size of the splitting. The analytical study also was preformed by using multipole expansion on Lennard-Jones potential in order to gain a more physical perspective on confined quantum molecular degree of freedom.

Acknowledgements

The reason this paper can be completed is because I stood on the shoulders of many great people. Rain or shine these people helped me and believed in me. Through thick and thin these people never complained, never lost faith. Here I wish to acknowledge them, may their tireless support never go unnoticed.

To Prof. Michel Gingras and Prof. Pierre-Nicholas Roy, I would like to express my deepest gratitude. Thank you both, for always been the first to provide priceless guidance, more often than not in the nick of time too. Thank you both for always been the first to give me aid no matter how late it got, and replying to all my emails regardless of the nature of the questions asked. And finally, thank you both, for been there for me when everything went south.

To Prof.Marcel Nooijen, thank you for been part of this project, and for providing me with valuable and often extremely enlightening pointers.

To my colleague Dr.Jeff Rau. Whether you do it intentionally or not, you often provided me with a spark of inspiration so profound, that I am usually dumbfounded by your genius. Of course more often than not, you would get the spark of inspiration yourself and then tirelessly try to explain and make me understand what just happened. Without your help, and the miles of equations you wrote for me, this project would not have gotten very far. Thank you.

To my colleague Spencer Yim. As with everything in life, a good foundation is key to success. Thank you for providing me with an extremely good foundation for my project when I first started it all. To my colleague Dmitri Iouchtchenko. Thank you for helping me with any and every computer related issues. Your support is more important to me than you could possibly imagine. I would also like to thank: Brian Yee, Cyrus Xu Cerkauskas, Xiaolong Zhang, Ce Zhou, Weiqiang Fu, Qianshi Wei,Tom Halverson, Yulia Kalugina, Matthew Schmidt and Kevin Bishop for many stimulating and enlightening conversations as well as all my colleagues in Prof. Michel Gingras and Prof. Pierre-Nicholas Roy group. Lastly, I want to thank Hunt Xu for improving the appearance of this paper, all my friends for their encouragement, and my family for their warmth and understanding.

Dedication

This is dedicated to people I love.

Table of Contents

List of Tables ix

List of Figures xi

1 Introduction 1

1.1 A Brief Review of C_{60} . . . 2

1.1.1 Chemical Bonding . . . 2

1.1.2 Icosahedral Symmetry Operations . . . 2

1.1.3 Electronic States . . . 4

1.1.4 Vibrational Modes . . . 5

1.1.5 Crystalline Structure . . . 5

1.2 Background of Confined Quantum Molecule . . . 7

1.2.1 A Brief Summary on General Confined Molecule . . . 7

1.2.2 Crystalline Structure of $H_2@C_{60}$ . . . 8

1.2.3 Quantum Dynamics of $H_2@C_{60}$ . . . 9

1.3 Motivation and Objective . . . 10

1.4 Outline of the Thesis . . . 12

2 Model **14**

2.1 Hamiltonian . . . 15

2.2 Rotational Motion . . . 15

2.3 Translational Motion . . . 16

2.4 The Potential Energy Surface(PES) . . . 17

2.4.1 Previous Studies on the PES . . . 17

2.4.2 Lennard-Jones potential . . . 18

3 Method **21**

3.1 Matrix Elements . . . 22

3.2 Basis Size Truncation . . . 23

4 Exact Diagonalization Results **25**

4.1 The "intra-cage" Interaction is the Main Reason of Splitting . . . 26

4.2 Sensitivity Analysis of Splitting on C_{60} geometry . . . 29

4.3 Translational and Rotational Coupling . . . 31

5 Analytical Approach **34**

5.1 A Brief Summary of Multipole Expansion for Electric Potential . . . 35

5.2 Multipole Expansion on L-J of Pinned H_2 . . . 36

5.2.1 Formalism . . . 36

5.2.2 Validation . . . 37

5.3 Multipole Expansion on L-J of Unpinned H_2 . . . 41

5.3.1 Formalism . . . 41

5.3.2 Validation . . . 44

6 Conclusion **49**

6.1 Conclusion of Present Work 49

6.2 Future Directions 50

6.2.1 More Precise Potential 50

6.2.2 Dipolar Molecule Confined Inside C_{60} 51

References **52**

List of Tables

1.1 The table of general position of C_{3i} point group 9

1.2 The table of general position of for (x,y,z) in symmetry group $Pa\bar{3}$ . . 9

1.3 The splitting size observed in the inelastic neutron scattering experiment[40] 11

2.1 Parameters specifying potential energy surface:$\epsilon(cm^{-1})$ and $\sigma(\mathring{A})$ are L-J potential parameters, w is a dimensionless weight as discussed in the text. [57] 19

2.2 Parameters specifying potential energy surface:$\epsilon(cm^{-1})$ and $\sigma(\mathring{A})$ are L-J potential parameters,w is a dimensionless weight as discussed in the text,and ν is the vibrational quantum number to specify the rotational constant B_ν.[57] 19

4.1 The C_{60} geometry in orientationally ordered phase given in [20]. . . . 26

4.2 The splitting of ortho-H_2(J=1) ground state for PES2ν0 28

4.3 The splitting of ortho-H_2(J=1) ground state for OPESν1 28

4.4 The splitting of ortho-H_2(J=1) ground state for OPESν0 28

4.5 Von Neumann entanglement entropy of ortho-H_2 state calculated using OPESν1: $|\Phi = 1\rangle$ is the first eigenfunction of ortho-H_2 and the basis function is expressed in the form $|n_x n_y n_z; lm\rangle$ 33

4.6 Von Neumann entanglement entropy of ortho-H_2 state calculated using PES2ν0: $|\Phi = 1\rangle$ is the first eigenfunction of ortho-H_2 33

5.1 The tabulation of multipole term(Q_{lm}) with PES2 that gives negative splitting 39

5.2 The tabulation of multipole term(Q_{lm}) with PES2 that gives positive splitting 39

5.3 The tabulation of multipole term(A_{lm}) with PES2ν0 that gives negative splitting. 44

5.4 The tabulation of multipole term(A_{lm}) with PES2ν1that gives positive splitting 45

5.5 The tabulation of multipole term (A_{lm}) with OPESν1 that gives negative splitting 47

5.6 The tabulation of multipole term (A_{lm}) with OPESν1 that gives negative splitting. 48

List of Figures

1.1 Molecular structure of the C_{60} 2

1.2 A demonstration of three kinds of rotational symmetry in molecule C_{60}: left is the twofold axis, middle is the threefold axis, and right is the fivefold axis. 3

1.3 Electronic energy levels of C_{60} from spherical symmetry to Ih symmetry [26] 4

1.4 A illustration of the p-phase and h-phase relative neighbouring C_{60} molecular orientation: grey part from one cage blue part from its nearest neighbour 6

1.5 The demonstration of three endofullerene [35, 30, 31] 8

1.6 The illustration showing that the three-fold degeneracy can be lifted in opposite order: S>0 and S<0 12

2.1 1D potential $V(x)$ cuts along x of H_2 inside C_{60} of PES2 (Left) and OPES (Right): solid line and dash line stands for H_2 perpendicularly and parallel move along C_2 axis of C_{60} [57] 20

4.1 Diagrammatic representation of a H_2 sitting in different cage environments. 27

4.2 The sorted splitting (S) (cm^{-1}) varies from cage to cage in over 40 random distorted cages with C_{3i} symmetry on PES2 (Left) and OPES (Right): (a) red circle and blue square are splitting with H_2 in its vibrational ground state and first excited state. (b) The difference of splitting with H_2 in its vibrational ground state and first excited state. 30

4.3 The comparison of splitting with different truncated basis on PES2ν0 (Left) and OPESν1 (Right): difference between S_{full} and S_{ED0} and difference between S_{PT} and S_{ED0}. 32

5.1 The comparison of potential dependence on $\cos\theta$ between multipole expansion (red line) and accumulation 2-site L-J potential (blue line): Left potential gives negative splitting order and right one gives positive splitting order. 38

5.2 The comparison between analytical approach and numerical calculation for pinned rotor with PES2: The S_{PT} is the splitting calculated by exact diagonalization in ortho-H_2 ground state(J=1), which is the first order degeneracy perturbation theory given by $\langle 1M'|\, V\, |1M\rangle$. The $S_{multipole}$ is the splitting calculated by multipole expansion by using Equation 5.13. 40

5.3 The comparison of potential dependence on $\cos\theta$ between multipole expansion (red line) and L-J potential (blue line) for unpinned H_2 with PES2ν0: Left potential gives negative splitting order and right one gives positive splitting order. 45

5.4 The comparison of block diagonalization calculation and multipole expansion calculation on PES2ν0. 46

5.5 The comparison of potential dependence on $\cos\theta$ between multipole expansion (red line) and L-J potential (blue line) for unpinned H_2 with OPESν1: Left potential gives negative splitting order and right one gives positive splitting order. 47

5.6 The comparison of block diagonalization calculation and multipole expansion calculation on OPESν1. 48

Chapter 1

Introduction

The endofullurene $H_2@C_{60}$, first synthesized in 2005, has since become a classical model in the study of quantum dynamics of a single confined molecule. Recently, $H_2@C_{60}$ has drawn great attention because of the coupled translational and rotational motion of H_2 when confined inside C_{60}. In this Chapter, an outline of the fascinating features of C_{60} will be presented including chemical bonding, symmetry operations, electronic states and vibrational modes of the C_{60} molecule. A general introduction on the crystalline structure of crystalline C_{60} will also be provided as it is the same as that of $H_2@C_{60}$. A summary on the symmetry group $Pa\bar{3}$ will be presented as it will closely relate to our work. Finally, the fundamental research motivation and objective of this work and the outline of the structure of this thesis will be discussed.

1.1 A Brief Review of C_{60}

1.1.1 Chemical Bonding

The Buckminsterfullerene has the chemical formula of C_{60}, was discovered in 1985 [34], and is a nearly spherical fullerene molecule. This molecule is also known as buckyball or soccer ball. C_{60} contains 12 pentagons and 20 hexagons. This means that there are 60 vertices for the carbon atoms sharing 90 covalent bonds between them, 30 electron-rich double bonds, and 60 electron-poor single bonds [44]. The pentagon is made of 5 electron poor single bonds and the hexagon is made of 3 single bonds and 3 double bonds as shown in Figure.1.1. C_{60} has a cage-like truncated icosahedron structure and has been described as the roundest molecule that can possibly exists by Curly and Smalley [19, 33]. The nucleus to nucleus diameter of C_{60} molecule is around 10.1Å and the length of a single bond that connects two hexagons is slightly larger than that of a double bond which connects two pentagons. The average bond length of a C_{60} molecule is about 1.4 Å**??**. C_{60} molecule in gas phase belongs to the icosahedral (Ih) symmetry group [19, 43].

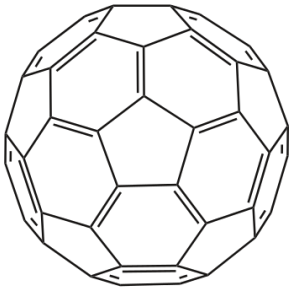

Figure 1.1: Molecular structure of the C_{60}

1.1.2 Icosahedral Symmetry Operations

C_{60} molecule is highly symmetrical and there are many transformations that map the C_{60} molecule back onto itself. These transformations are rotation around an

axis, reflection about a plane and inversion with respect to a point. All rotational axes and mirror planes must go through the centre of mass of C_{60} since the centre of mass of the C_{60} molecule must be unchanged under all symmetry operations. There are three kinds of rotational symmetry for a C_{60} molecule as shown in Figure.1.2. One is 2-fold axis through the centres of the edges between two hexagons which is

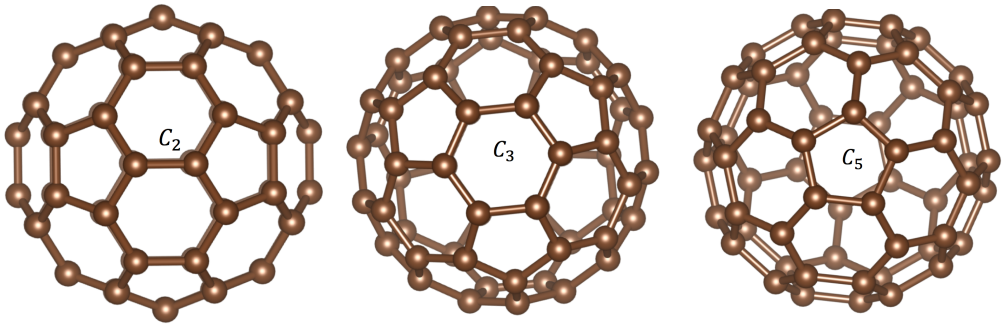

Figure 1.2: A demonstration of three kinds of rotational symmetry in molecule C_{60}: left is the twofold axis, middle is the threefold axis, and right is the fivefold axis.

referred to as C_2 axis. There are 30 edges between two hexagons since each hexagon is neighboured by three other hexagons. As a result, there are 15 distinct 2-fold axes in one C_{60} molecule. The second one is 3-fold axis through the centre of two facing hexagons, a rotation of 120 degrees about this axis is needed to map the molecule onto itself. Since each axis passes through two hexagons, 20 hexagons in one C_{60} molecule will gives 10 different 3-fold axes which are referred to as C_3 axes. The third one is 5-fold rotational axis through the centre of two facing pentagons, a rotation of 72 degrees about this axis will map the molecule onto itself. 12 pentagons in C_{60} molecule will give 6 different 5-fold rotational axes which are referred to as C_5 axes. The reflection symmetries are in the planes that contain two edges between adjacent hexagons. There are also 15 different mirror planes. Finally, C_{60} has inversion symmetry with respect to its centre of mass. It means that one can replace each carbon atoms' coordinate (x, y, z) by $(-x, -y, -z)$, with the C_{60} molecule mapping back onto itself. All these symmetry operations form the Ih point group. Symmetry consideration is very important when dealing with physical problems with fullerenes

such as the electronic states or vibrational modes. The spherical harmonics are treated as natural basis functions for the full rotational group.

1.1.3 Electronic States

In this subsection, we consider the electronic states of C_{60} fullerene molecules within a very simple description. Initially, C_{60} was assumed to be a perfect sphere. However, qualitative treatment adapted from the quantum mechanics of one-electron hydrogen atom gives electronic structure with unpaired electrons [19, 43, 44]. This is in a contradiction with the fact that C_{60} is an insulator and has no unpaired electrons. This contradiction gets resolved if the symmetry is lowered from spherical to Ih since all unpaired electrons become paired under the Ih symmetry. As

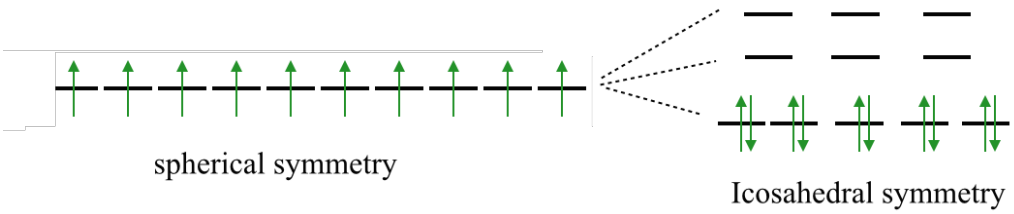

Figure 1.3: Electronic energy levels of C_{60} from spherical symmetry to Ih symmetry [26]

shown in Figure.1.3, if C_{60} has spherical symmetry, each carbon is single bonded to three other carbons using three of four valence electrons with the remaining one electron for each carbon moving on the sphere that is created by the 60 carbon atoms. This qualitative treatment of 60 delocalized electrons moving on a sphere results in 10 unpaired electrons. After the symmetry is lowered to Ih, the highest occupied molecular orbital is fivefold degenerate and the lowest unoccupied molecular orbital is threefold degeneracy. The existence of two triply degenerate sates shown in Figure.1.3 is consistent with the experimental results showing that K_3C_{60} is a conductor while K_6C_{60} is an insulator [52].

1.1.4 Vibrational Modes

Symmetry consideration is also very important to characterize the nature of the vibration modes of C_{60} molecule. In this subsection, we briefly summarize the symmetries of the vibrational modes for C_{60} molecule. After one subtracts the translational and rotational degree of freedom, there remains 174 vibrational degrees of freedoms. However, due to the high symmetric of Ih symmetry, many vibration modes are degenerate and only 46 distinct vibrational frequencies remain. They correspond to the following symmetry decomposition [12, 13, 44]:

$$2A_g + 3F_{1g} + 4F_{2g} + 6G_g + 8H_g + A_u + 4F_{1u} + 5F_{2u} + 6G_u + 7H_u. \quad (1.1)$$

The coefficients can be explained as follows: $2A_g$ means that two distinct eigenfrequencies have A_g symmetry while $3F_{1g}$ means three distinct eigenfrequencies have F_{1g}, etc. The lowest frequency modes of A_g is so called the "breathing" mode and refers identical radial displacements for all 60 carbon atoms. The frequency of this mode is about $450cm^{-1}$[12, 29] and the root-mean-square displacement at zero temperature is 0.04 Å[29].

1.1.5 Crystalline Structure

In this subsection, we review features of the crystalline structure of C_{60} including the crystal structure of C_{60} at room temperature, the structural phase transition of temperature dependence and the neighbouring orientation feature of C_{60} [12]. In solid state, C_{60} molecules will crystallize into face centred cubic (FCC) lattice structure. The lattice constant is 14.17Å and the nearest-neighbour C_{60}-C_{60} distance is 10.02 Å [12, 50] at room temperature and ambient pressure [12]. The C_{60} molecules are located at the lattice points of a FCC lattice with one C_{60} molecule per primitive FCC unit cell or four molecules per simple cubic (SC) unit cell. C_{60} displays a structural phase transition as a function of temperature. At room temperature, C_{60} molecules are rotating rapidly about their lattice positions. There is no orientational order and all molecules are treated as equivalent molecules. Consequently, the crystal structure of C_{60} is FCC and the space group symmetry at room temperature is

$Fm\bar{3}m$ as revealed by x-ray and neutron diffraction [12, 21, 15, 51]. The structural phase transition from FCC to SC structure occurs when the temperature decreases below a temperature T_1. This temperature is called characteristic temperature and is about 261 K. Below T_1, the C_{60} molecules only have one degree of freedom which is the rotational motion about the four $< 111 >$ direction due to the strong correlation with the adjacent molecules. As a result, the lattice structure of solid C_{60} is SC when the temperature is below T_1 and the symmetry of C_{60} is $Pa\bar{3}$. Moreover, as temperature goes below T_1, there exists two different phase in the idealized ordered structure with respect to the relative orientation of adjacent C_{60} molecules [12].

- p-phase: the electron rich double bonds faces the electron poor pentagon of the adjacent C_{60} molecule
- h-phase: the electron rich double bonds faces the electron rich hexagon of the adjacent C_{60} molecule

(a) p-phase (b) h-phase

Figure 1.4: A illustration of the p-phase and h-phase relative neighbouring C_{60} molecular orientation: grey part from one cage blue part from its nearest neighbour

As the temperature continues to decrease, another "phase transition" will occur at temperature T_2. This "phase transition" involves the transition between p-phase orientation and h-phase orientation [12, 13]. The value of T_2 is not determined since it differs from different properties being measured. A number of experiments such as: the velocity of sound [12, 32, 22], specific heat measurement [12, 18, 2, 47, 4], dielectric relaxation studies [12, 5] and neutron scattering measurement [12, 10], showed that this "phase transition" occurs at a temperature range of 90K-160K.

As temperature gets lower, most of the molecules tend to have a p-phase with the adjacent molecules since p-phase configuration has lower energy than that of h-phase configuration. Moreover, when $T_2 = 90K$, 87% of the intermolecular alignment are reported in lower energy p-phase and 17% of the intermolecular alignments are reported in slightly higher energy level h-phase [12]. This percentage will be maintained down to about 50K.

1.2 Background of Confined Quantum Molecule

1.2.1 A Brief Summary on General Confined Molecule

In this subsection, we present a brief summary on general endohedral compounds including several current achieved cases, the method to synthesize those compounds, and application of the endohedral compounds. Endohedral compounds are when a guest atom or molecule is trapped in the interior of a host molecule. The first endohedral compounds obtained by trapping single lanthanum atom inside carbon cage which was denoted as $La@C_{60}$[7, 16]. This notation can be explained as the following: the atom or molecule on the left of @ will be assumed to be the guest molecule and all atoms listed on the right will be assumed to be part of the cage [7]. The host molecule usually are fullerenes, such as C_{60}, C_{70} and C_{80} and in this case the endohedral compounds is also called endofullerene. The endofullerene was synthesized by a procedure named "molecular surgery" [36, 30]. "Molecular surgery" involves using a series of chemical reactions to open a hole on the cage, trapping the guest molecule inside and preforming another series chemical reactions to close the hole. The endofullerene $H_2@C_{60}$ in Figure.1.5a where a small H_2 molecule that is encapsulated into a fullerene cage C_{60} was the first to be synthesized. [30] Similar molecules such as: $H_2O@C_{60}$ [35] in Figure.1.5b and $HF@C_{60}$ in Figure.1.5c have also been synthesized since[31]. One important reason that motivated people to synthesize $H_2@C_{60}$ endofullerene is the need to storage clear H_2 as it is an ideal fuel and in principle reduces or even eliminates CO_2 emissions[48, 42]. Moreover, in order

(a) $H_2@C_{60}$ (b) $H_2O@C_{60}$ (c) $HF@C_{60}$

Figure 1.5: The demonstration of three endofullerene [35, 30, 31]

to reveal the fundamental properties of water molecules that exist in non-hydrogen-bonding environments, the endofullerene $H_2O@C_{60}$ is also necessary[28]. All these three endofullerene displays remarkable quantum effects where the translational and rotational motion becomes coupled due to the confinement. In our project, we focused on $H_2@C_{60}$

1.2.2 Crystalline Structure of $H_2@C_{60}$

The crystalline structure of $H_2@C_{60}$, including the crystal structure at room temperature, the structural phase transition of temperature dependence, and the neighbouring orientation feature are all same with that of C_{60}. In this subsection,we will emphasis the structure feature when the lattice structure is in the symmetry group $Pa\bar{3}$ in which the point group of a single C_{60} molecule is C_{3i}. The C_{3i} operator involves the following 3-fold rotation and inversion shown in Table 1.1. For a single C_{60} molecule that has C_{3i} symmetry, only 10 independent carbon atoms' positions are needed in order to obtain any carbon atoms position in one C_{60} molecule. Starting with these 10 independent carbon atoms' positions, one can apply 3-fold rotation to get 30 rotational symmetry related carbons' position which are presented in left column of Table 1.1. Then by using inversion symmetry, one can obtain the 60 carbon atoms' position for one C_{60} molecule. The symmetry group $Pa\bar{3}$ involves the

3-fold Rotation	Inversion
(x,y,z)	(-x,-y,-z)
(z,x,y)	(-z,-x,-y)
(y,z,x)	(-y,-z,-x)

Table 1.1: The table of general position of C_{3i} point group

following transition in the space for all the C_{3i} general positions. Let us use (x,y,z) position as example as showing in Table 1.2. Similar transitions on (z,x,y), (y,z,x)

-x+1/2,-y,z+1/2
-x,y+1/2,-z+1/2
x+1/2,-y+1/2,-z

Table 1.2: The table of general position of for (x,y,z) in symmetry group $Pa\bar{3}$

and their inversions also needs to form the full group of positions of $Pa\bar{3}$ symmetry. In summary, the crystalline structure of $H_2@C_{60}$ is the same as that of C_{60}. In the temperature regime that relates to our projects, $H_2@C_{60}$ is in symmetry group $Pa\bar{3}$ in which the single C_{60} has C_{3i} symmetry.

1.2.3 Quantum Dynamics of $H_2@C_{60}$

The remarkable quantum effects of coupled transitional and rotational degrees of freedom will play an important role once the H_2 is trapped into the C_{60}. The quantum dynamics of H_2 confined in C_{60} is even more attractive since H_2 molecules has two spin isomers, which are para-H_2 and ortho-H_2[8]. For para-H_2, it gives the antisymmetric total spin($I = 0$) isomer and has antiparallel spins , while for ortho-H_2, it gives the symmetric total spin ($I = 1$) isomer and has parallel spins.The Pauli exclusive principle requires that the total wave function to be antisymmetric with respect

to the exchange of nuclei due to the fact that the H nuclei spins are fermions. In the Born-Oppenheimer approximation, If we ignore the rotation-vibration coupling, the total wave function of the H_2 can be written as:$|\Psi\rangle = |\psi_s\rangle \cdot |\psi_{\text{el}}\rangle \cdot |\psi_{\text{vib}}\rangle \cdot |\psi_{\text{rot}}\rangle$ which is referring to the nuclei spin, electronic, vibrational and rotational wave functions. The vibrational and electronic wave function are symmetric with respect to permutation of the two hydrogen molecules. Consequently, For para-H_2, only even rotational quantum numbers are allowed $j = 0, 2, 4, 6...$,while for the ortho-H_2, only odd rotational quantum number are allowed $j = 1, 3, 5, 7...$ in order to have an antisymmetric wave function. In our work, we will refer $j = 1$ state to ortho-H_2 ground state. The spin conversion between the two isomers are extremely slow with the absence of magnetic impurities and dopants since no measurable para-H_2 and ortho-H_2 conversion in pure solids has been observed in several days at cryogenic temperature [12]. In summary, para-H_2 and ortho-H_2 can be treated as two different physical spices inside the cage C_{60}.

1.3 Motivation and Objective

Due to the fascinating quantum dynamic features of the endofullerene, $H_2@C_{60}$ has aroused extensive interests both in theoretical [56, 57, 53, 58, 17, 59, 14]. Numerous experimental studies such as: nuclear magnetic resonance [6] and inelastic neutron scattering [25, 24, 23, 54, 40] have been reported. In this section, we will present the motivation as well as the objective of this work. The coupled translational and rotational motion of H_2 inside C_{60} would be effected by the potential energy surface that H_2 molecule experiences due to the confinement. The energy spectrum of confined H_2 will be related to the symmetry of this potential energy surface which would directly relate to the symmetry of C_{60}. As we mentioned before, in gas phase, a single C_{60} molecule has icosahedral (Ih) symmetry, and the rotational motion of H_2 preserved the high degeneracy up to J=5 under Ih symmetry [13, 12]. This splitting principle has been justified by the following theoretical works [56, 57, 53, 58]. In its solid state, C_{60} molecules crystallize into cubic lattice with space group $Pa\bar{3}$[20] and

the symmetry of a single C_{60} molecule will decrease from Ih to C_{3i}. The rotational three-fold ortho-H_2 ground state($j = 1$) will split into two doubly degenerate level and single nondegenerate level due to the nature of C_{3i} symmetry. This splitting principle was also observed by the most recent inelastic neutron scattering experimental result in Ref.[40]. These experiments were preformed in the temperature range where C_{60} has $Pa\bar{3}$ symmetry. The splitting of three-fold ortho-H_2 ground state($j = 1$) was studied as a function of temperature from 40K down to 60 mK. It demonstrated that the three-fold degeneracy of ortho-H_2 ground state could split into a low energy nondegeneracy level and a high energy doubly degeneracy level [40]. This experiment also found that the size of this splitting would depend on orientation of the C_{60} molecule. More specifically, the splitting size depend on the statistical weights of p-phase and h-phase neighbouring orientation C_{60} molecules as showing in Table.1.3[40]. The "p-phase rich" means that statistical weights of

	p-phase rich	h-phase rich
S	1.089cm^{-1}	1.371cm^{-1}

Table 1.3: The splitting size observed in the inelastic neutron scattering experiment[40]

p-phase orientation is larger than that of the h-phase orientation and the "h-phase rich" means that statistical weights of h-phase orientation is larger than that of the p-phase orientation. Moreover, we will use "S" to represent the splitting and use wavenumber (cm^{-1}) as the unit of splitting in this work as showing in Table.1.3. Here we will clarify the sign of "S" due to the fact that we also found that the three-fold degeneracy can be lifted in opposite order. Therefore, we will use a positive "S" to denote that the splitting had the same order as the experimental result. The sign of splitting "S" have the following notation:

- S>0: the three-fold degeneracy of rotational ortho-H_2 ground state ($j = 1$)splits into a low energy nondegeneracy level and a high energy doubly degeneracy level

- S<0: the three-fold degeneracy of rotational ortho-H_2 ground state ($j = 1$) splits into a high energy nondegenerate level and a low energy doubly degenerate level

These notations are illustrated in Figure.1.6

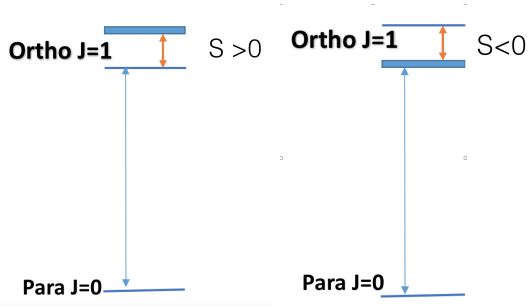

Figure 1.6: The illustration showing that the three-fold degeneracy can be lifted in opposite order: S>0 and S<0

The fundamental origin that responsible for the listing of the three-fold degeneracy is still an open problem in chemical physics. There are two possibilities and here we will use the notations used in Ref.[40]. The one possibility is that it could be caused by the interaction between H_2 and its own cage. This will be refer to as "intra-cage" interaction. The other one is the interaction between $H_2@C_{60}$ and neighbouring $H_2@C_{60}$ molecules. This will be refer to as "inter-cage" interactions. The objective of this work is to gain insights into the role of inter-cage or intra-cage interactions in determining the energy spectrum of H_2. Furthermore, the splitting size of the three-fold degeneracy of rotational ortho-H_2 ground state ($j = 1$).

1.4 Outline of the Thesis

This concludes the introduction of this thesis, which was aimed to give the reader a general understanding of small molecules confined inside C_{60}. The remaining part of this work consists of four chapters. Chapter 2 will introduce the model

used to accomplish our objective. The primary focus of Chapter 2 is a physical understanding of H_2 confined into C_{60}. It will start with a model of a free rotor, then add translational degree of freedom and finish by adding potential energy surface between H_2 and C_{60}. Chapter 3 will provide the numerical techniques required to investigate our problem. It will present the method of exact diagonalization, the matrix element and a discussion of the effect of the basis size truncation. Chapter 4 will display the results of applying the methods presented in Chapter 3 on the Hamiltonian of H_2 confined inside C_{60} with the potentials discussed in Chapter 2. In order to develop a more efficient method as well as understand the physical meaning, we will introduce an analytical perspective to solve our problem in Chapter 5 and Chapter 6. Chapter 5 will introduce the analytical method on a toy model. After the validation of the toy model in Chapter 5, Chapter 6 will present the analytical method on the real model that was introduced in Chapter 2. This model leaves future direction of our work with additional further corrections on the potential between H_2 and C_{60}. With the understanding of the endofullerene $H_2@C_{60}$, the process of understanding the physical perspective of other endofullerene such as $H_2O@C_{60}$ or $HF@C_{60}$ would be easier. The possible directions of future work will be discussed in Chapter 7.

Chapter 2

Model

In this chapter, we start with stating all assumption basing on the quantum nature of small molecule H_2 trapped inside a fullerene cage C_{60} and presenting the full Hamiltonian that consists of translational part, rotational part as well as interaction part. Then we will introduce each part of the Hamiltonian as well as the natural basis function. A discussion on the potential energy surface will be present. Finally , we will give a brief summary on previous studies of the potential of H_2 confined inside C_{60}. We will present the L-J potential as well as its parameters we used to physically describe the interaction between H_2 and its cage C_{60}.

2.1 Hamiltonian

Considering the quantum nature of small molecule H_2 trapped inside a nano cavity C_{60}, there are several features that needs to be emphasized in order to simplify the Hamiltonian and solve the problem. First, C_{60} is treated as a rigid cage due to fact that the H_2-C_{60} interaction is much weaker than the lowest frequency mode of C_{60} molecule [56]. The couplings between them are very weak and it is measured by the Raman and infrared spectra [11]. Second, C_{60} is treated as non-rotating molecules due to the fact that the three rotational constants of C_{60} are equal to $2.803 \times 10^{-3}\text{cm}^{-1}$and are negligible when compared to the H_2-C_{60} interaction [59]. Third, H_2 is treated as a rigid rotor, which is justified by the fact that vibrational motion of H_2 is coupled very weakly to the coupled translational and rotational motion [59]. With assumptions shown above, the coupled translational and rotational motion of H_2 inside C_{60} can be described by a 5D coordinate system (x, y, z, θ, ϕ). Finally the 5D Hamiltonian of rigid H_2 trapped inside a rigid and non-rotating C_{60} cage can be written as follows [59]:

$$H = -\frac{\hbar^2}{2\mu}\left(\frac{\partial^2}{\partial x^2} + \frac{\partial^2}{\partial y^2} + \frac{\partial^2}{\partial z^2}\right) + B_\nu \mathbf{L}^2 + V(x, y, z, \theta, \phi). \tag{2.1}$$

2.2 Rotational Motion

The rotational motion is described by θ and ϕ, which specify the orientation of H_2 with respect to C_{60} cage frame. The Hamiltonian for rotational part has the following form:

$$H_{\text{rot}} = B_\nu \mathbf{L}^2. \tag{2.2}$$

$\mathbf{L}^2$ is the angular momentum operator of diatomic H_2 molecule, and is used to describe the rotational motion of H_2. B_ν is the rotational constant of the H_2 in vibrational ν state and the value is given by $B_\nu = B_{\text{eq}} - \alpha(\nu + 1/2)$ where α is a vibration-rotation interaction constant. The equilibrium rotational constant $B_{\text{eq}} = 59.3\text{cm}^{-1}$ and the vibration-rotation constant $\alpha = 2.98\text{cm}^{-1}$ are measured

from IR spectra of H_2@C_{60} [38]. The rotational basis function used in this work is spherical harmonic wavefunction since $|l, m\rangle$ are eigenfunction of $\mathbf{L}^2$simultaneously:

$$\mathbf{L}^2 |l, m\rangle = l(l+1) |l, m\rangle , \quad \text{with } |l, m\rangle \equiv Y_{lm}(\theta, \phi). \tag{2.3}$$

Since this study is focused on the degeneracy lifting of ortho-H_2 ground state ($l = 1$) manifold, the spherical harmonic function Y_{1m} under spherical coordinates(θ, ϕ) will be listed.

$$Y_{1,0} = \sqrt{\frac{3}{4\pi}} \cos\theta$$
$$Y_{1,-1} = \sqrt{\frac{3}{4\pi}} \sin\theta e^{-i\phi}$$
$$Y_{1,1} = -\sqrt{\frac{3}{4\pi}} \sin\theta e^{i\phi}$$

Finally, as mentioned in 1.2.3, H_2 can exist as two nuclear spin isomers ortho-H_2 and para-ceH2. Due to the fact that the conversion between the two spin isomer is extremely slow, one can treat ortho-H_2 and para-ceH2 as two distinct physical species. It will dramatically decrease the basis size of the full Hamiltonian and save numerous computational expenses.

2.3 Translational Motion

In addition to rotating, H_2 has translational degree of freedom and can be described by 3D coordinate system(x, y, z). In this system, x, y and z specify the centre of mass (CM) position of H_2 away from the geometry centre of C_{60}. The Hamiltonian for rotational part has the following form:

$$H_{\text{trans}} = -\frac{\hbar^2}{2\mu} \left(\frac{\partial^2}{\partial x^2} + \frac{\partial^2}{\partial y^2} + \frac{\partial^2}{\partial z^2} \right). \tag{2.4}$$

In the above Equation 2.4, $-\frac{\hbar^2}{2\mu}\frac{\partial^2}{\partial x^2}$ describes the translational motion of the CM of H_2 along x direction. μ is the reduced mass of H_2 inside C_{60}, which is given by the

mass of H_2 and C_{60} with $\frac{m_{H_2} m_{C_{60}}}{m_{H_2}+m_{C_{60}}}$. Due to the large mass difference between H_2 and C_{60}, the reduced mass of H_2 is only slightly smaller than the mass of H_2(2.0160amu). The value of 2.0104amu will be used in this work to represent it. The 3D harmonic oscillator wave-function for translational motion of CM of H_2 coupled with spherical harmonics for rotational motion are used in this work in order to preform exact diagonalization on the Hamiltonian. The basis function can be written as follows:

$$\Psi(x, y, z, \theta, \phi) = \langle x, y, z, \theta, \phi | \left(|n_x, n_y, n_z\rangle \otimes |l, m\rangle \right). \tag{2.5}$$

$|n_x, n_y, n_z\rangle$ is the 3D harmonic oscillator eigenfunction and $|n_x\rangle$ (similar with $|n_y\rangle$ and $|n_z\rangle$) can be written under the cartesian coordinate basis as follows:

$$|n_x\rangle = \phi_{n_x}(x) = \frac{1}{\sqrt{2^n n!}} \left(\frac{m\omega}{\pi\hbar}\right)^{1/4} \exp\left\{-\frac{m\omega x^2}{2\hbar}\right\} H_n\left(\sqrt{\frac{m\omega}{\hbar}} x\right). \tag{2.6}$$

$H_n(x)$ is the n-th order Hermite polynomials. The choice of using the 3D harmonic oscillator eigenfunction basis function is motivated by the potential of the problem, and can be approximated by a harmonic potential at the vicinity of the equilibrium point.

2.4 The Potential Energy Surface(PES)

2.4.1 Previous Studies on the PES

In order to describe the H_2 that trapped inside C_{60}, now we need to come up with an effective potential that characterizes the interaction between the trapped molecule H_2 and its cage C_{60}. A number of experimental measurements have been performed using spectroscopic techniques such as nuclear magnetic resonance spectroscopy (NMR), inelastic neutron scattering (INS), and infrared (IR) spectroscopy. An excellent review on IR, INS and NMR spectroscopy of $H_2@C_{60}$ at cryogenic temperature was presented by Mamone [39]. After obtaining energy levels of $H_2@C_{60}$ by using all three of the aforementioned spectroscopic techniques, there exist two choices to formalize the PES. One was that the PES could be obtained as a sum

of the two body interactions over all carbon and hydrogen atoms and fitted to the experimental measured spectrum to parameterize the potential. A standard two-site Lennard-Jones potential was first used to fit the energy level of H_2 in C_{60} cage [38, 37]. To get a better fitting, a three-site LJ potential, which also accounts for the interactions between the centre of mass of H_2 and all carbon atoms was proposed later by fitting IR spectra [38]. This was motivated by the molecular charge distribution which was located not only at the exact nuclear positions, but also in the intermediate region between the hydrogen atoms. Consequently, the three-site potential improved the accuracy of the spectrum fitting, especially for higher energy levels. In summary, principally, a real potential energy surface that characterizes the interaction between H_2 and C_{60} is required. However, considering the complexity of coming up with a real potential, and that since empirically parameterizing 5D Lennard-Jones(L-J) potential gives good agreements with the IR spectroscopic measurements, [38, 37], we will use a 5D parameterized L-J potential to describe the interaction between trapped H_2 and C_{60}.

2.4.2 Lennard-Jones potential

The 5D potential $\mathrm{V(x, y, z, \theta, \phi)}$ can be written in L-J form:

$$V = \sum_{j=1}^{2} \sum_{i=1}^{60} V(r_{ij}) + \mathrm{w} \sum_{i=1}^{60} V(r_{im}) \tag{2.7}$$

In Equation.2.7, r_{ij} is the distance between i-th hydrogen atom of H_2 and j-th carbon atom of C_{60}. r_{im} is the distance between CM of H_2 and j-th carbon atom. w is a dimensionless weight parameter that efficiently changes the L-J potential energy surface. In Equation.2.7, the L-J potential $V(r)$ has the following form:

$$V(r) = 4\epsilon \left[\left(\frac{\sigma}{r} \right)^{12} - \left(\frac{\sigma}{r} \right)^{6} \right]. \tag{2.8}$$

In Equation2.8, ϵ and σ are standard L-J potential parameters,where ϵ is the depth of potential well and σ is the finite distance where inter-particle potential equals to zero. The L-J parameters [57] used in this work are displayed in Table 2.2.

	$\epsilon(\text{cm}^{-1})$	$\sigma(\text{Å})$	w
OPES	2.99	2.95	7.5
PES2	19.2	3.08	0.0

Table 2.1: Parameters specifying potential energy surface:$\epsilon(\text{cm}^{-1})$ and $\sigma(\mathring{A})$ are L-J potential parameters, w is a dimensionless weight as discussed in the text. [57]

When fitting with the IR spectroscopic measurements, besides the L-J parameters, the vibrational state of H_2 also play an important role in the behaviours of energy spectra. As suggested by [37], H_2 in vibrational ground state with PES2 is better fitting with IR spectra than it in excited vibrational state. While for H_2 with OPES, using H_2 in the first vibrational excited state can explain experimental measurements better than it in vibrational ground state[38]. The PES2 with H_2 in first vibrational excited state and the OPES with H_2 in vibrational ground state are two potential energy surfaces that are motivated by PES2ν0 and OPESν1 respectively. A detail explanation of vibrational quantum number ν can be found in 2.2. To get a

	$\epsilon(\text{cm}^{-1})$	$\sigma(\text{Å})$	w	ν
OPESν0	2.99	2.95	7.5	0.0
OPESν1	2.99	2.95	7.5	1.0
PES2ν0	19.2	3.08	0.0	0.0
PES2ν1	19.2	3.08	0.0	1.0

Table 2.2: Parameters specifying potential energy surface:$\epsilon(\text{cm}^{-1})$ and $\sigma(\mathring{A})$ are L-J potential parameters,w is a dimensionless weight as discussed in the text,and ν is the vibrational quantum number to specify the rotational constant B_ν.[57]

direct sense of the difference between the two kinds of potential energy surface,one can plot the potential with respect to the position of the centre of mass of the H_2 as shown in Figure.2.1. It is the plot given in [57]. The PES2 and OPES parameters generate very different well depths, and shapes of potentials that will effect the coupled translational and rotational motion of trapped H_2. However, as pointed out in

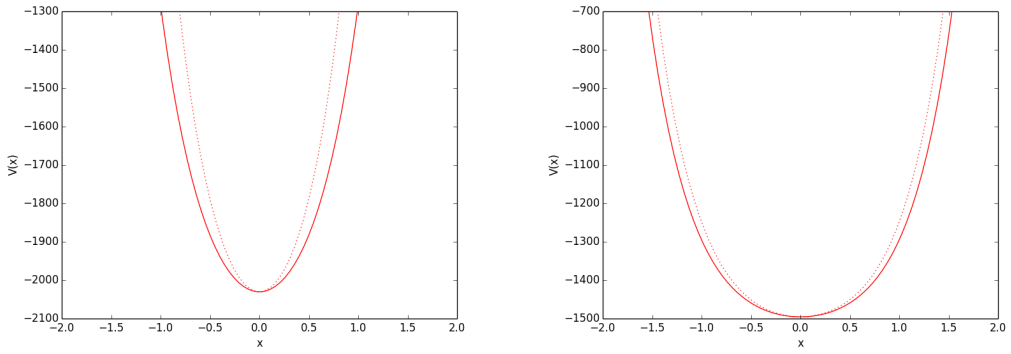

Figure 2.1: 1D potential $V(x)$ cuts along x of H_2 inside C_{60} of PES2 (Left) and OPES (Right): solid line and dash line stands for H_2 perpendicularly and parallel move along C_2 axis of C_{60} [57]

[55, 56, 57], the quantum translational-rotational dynamics of H_2/HD/D_2 in C_{60} on both potential energy surfaces all display the same patterns of degeneracies, which can be qualitatively understood in terms the model of the rigid rotor that is trapped inside a high symmetry cage with a large cavity. It is also shown that these features are robust, generic and independent of the details of the interaction potentials.

Chapter 3

Method

In this chapter, we introduce the methodology used to investigate the quantum rotor H_2 trapped inside C_{60} is exact diagonalization. The reason is that the time-independent Schrödinger equation is an eigenvalue problem. Even though the real physical problem is in the infinite dimensional space, the Schrödinger equation can be formulated as an eigenvalue matrix with the approximation of truncating Hilbert space to finite dimension. We will present the matrix element basing on the Hamiltonian and the basis functions that we defined in Chapter 2. Finally, a discussion on the basis size convergence will be provide, highlighting the convergence factor we used to proceed our project.

3.1 Matrix Elements

Having defined the Hamiltonian and the basis functions in Chapter 2, it is now possible to move with evaluating the matrix elements of the Hamiltonian under the basis functions. As mentioned before, the potential used in this work has harmonic potential behaviour in the vicinity of the equilibrium point. This point will be the geometry centre of the C_{60} molecule. From these set of states, H_2 molecule can be treated as a quantum harmonic oscillator that oscillating around the equilibrium point in the harmonic like potential well. This suggests one can rewrite the Hamiltonian in terms of 3D quantum harmonic oscillator Hamiltonian by adding the potential term $\frac{1}{2}m\omega^2\mathbf{r}^2$ and subtract this term in the 5D interaction potential $V(x, y, z, \theta, \phi)$ latter. The total hamiltonian will be unchanged and has the following form:

$$H = H_{\mathrm{QHO}} + B_\nu \mathbf{L}^2 + V'(x, y, z, \theta, \phi), \tag{3.1}$$

where H_{QHO} and $V'(x, y, z, \theta, \phi)$ have the following form:

$$H_{\mathrm{QHO}} = -\frac{\hbar^2}{2\mu}\nabla^2 + \frac{1}{2}m\omega^2\mathbf{r}^2 \text{ and } \mathrm{V}' = \mathrm{V} - \frac{1}{2}\mathrm{m}\omega^2\mathbf{r}^2. \tag{3.2}$$

Here, a parameter ω is used and represents the angular frequency of the H_2 molecule. The value of ω can be determined by the Taylor series expansion of potential V in terms of $\mathbf{r}$ around equilibrium position ($\mathbf{r}$=0), and more specifically by the second derivative of the potential. The value of the parameter ω will not effect the energy spectrum when using a converged basis size since the same quantities are added and subtracted. The matrix elements of H_{QHO} hamiltonian are easy to evaluate since it is the diagonal in the 3D quantum harmonic oscillator basis set.

$$\langle n_x, n_y, n_y| \, H_{\mathrm{QHO}} \left|n'_x, n'_y, n'_z\right\rangle = \hbar\omega \left(\frac{3}{2} + n_x + n_y + n_z\right) \delta_{n_x,n'_x}\delta_{n_y,n'_y}\delta_{n_z,n'_z}. \tag{3.3}$$

Similarly, the rotational part $B_\nu \mathbf{L}^2$ is diagonal in the spherical harmonic basis:

$$\langle l'm'| \, B\mathbf{L}^2 \, |lm\rangle = l(l+1)\delta_{l,l'}\delta_{m,m'}. \tag{3.4}$$

We can now proceed to evaluate the matrix elements of the interaction potential, which can be done using the translational and rotational basis separately. The rotational part is as follows:

$$\begin{aligned}\langle L'M'|\, V' \,|LM\rangle &= \int_{-1}^{1} d\cos(\theta) \int_{0}^{2\pi} d\phi \, \langle L'M'|\, V' \,|\theta\phi\rangle \, \langle \theta\phi|LM\rangle \\ &= \sum_{\alpha}\sum_{\beta} \mathrm{w}_\alpha \mathrm{w}_\beta \;\; Y^*_{L'M'}(\theta_\alpha,\phi_\beta) V'(xyz,\theta_\alpha,\phi_\beta) Y_{LM}(\theta_\alpha,\phi_\beta). \end{aligned} \tag{3.5}$$

In Equation.3.5, w_α is Gauss-Legendre quadrature weights, which are used to evaluate the integral over the polar angle part and has the following general form:

$$\int_{-1}^{1} f(x)dx = \sum_i \mathrm{w}_i f(x_i).$$

The ω_β are equal spaced weights from 0 to 2π which is used to evaluate the integral over the azimuthal angle. The translational part needs to be calculated under the 3D quantum harmonic and it can be written as follows:

$$\begin{aligned}\left\langle n'_x, n'_y, n'_z \middle| V' \middle| n_x, n_y, n_z \right\rangle &= \int dx \int dy \int dz \, \left\langle n'_x, n'_y, n'_z \right|\, V' \,|xyz\rangle \, \langle xyz|n_x, n_y, n_z\rangle \\ &= \sum_{i,j,k} \mathrm{w}_i \mathrm{w}_j \mathrm{w}_k \;\; \phi^*_{n'_x}(x_i)\phi^*_{n'_y}(y_j)\phi^*_{n'_z}(z_k) \;\; V'(x_i,y_j,z_k) \;\; \phi_{n_x}(x_i)\phi_{n_y}(y_j)\phi_{n_z}(z_k). \end{aligned} \tag{3.6}$$

Again, in the above equation, $\mathrm{w}_i, \mathrm{w}_j$ and w_k are Gauss-Laguerre quadrature weights. By combining all of the above together, one obtains all matrix elements of the Hamiltonian shown in Equation.2.1 under the basis function in Equation.2.5. After completing this, one can perform exact diagonalization on the Hamiltonian to get the full energy spectrum.

3.2 Basis Size Truncation

In this work, there are three convergence related factors that need to be stressed. First is the choice of the quantum oscillator frequency ω, which can be calculated

through the second derivative of potential. The frequency used in exact diagonalization calculation is 9.673×10^{-4} in atomic units. The second factor is the number of grid points used to get a converged value of the 5D integral. The number of grid points for the translational motion xyz is 30 which means in Equation.3.6 $i, j, k = 1...30$. Similarly, for rotational motion θ and ϕ is 30 and 20 which means in Equation.3.5 $\alpha = 1...30$ and $\beta = 1...20$, respectively. The third factor is that based on all of the above convergency studies, a rigorous basis size convergence study must be performed. The basis for translational wavefunction is truncated at $n_x + n_y + n_z \leq 11$, and for rotational motion where only the ortho-H_2 wavefunction (odd J) are used is truncated at $J \leq 5$.

Chapter 4

Exact Diagonalization Results

In this chapter, we will present the exact diagonalizations results for $H_2@C_{60}$. Firstly, we will introduce and clarify all cases we considered to investigate the origin of the degeneracy lifting of ortho-H_2 ground state. Basing on the comparison between different case, we will draw an important conclusion, which is "intra-cage" interaction is the main reason of this degeneracy lifting. Then we will focus on one $H_2@C_{60}$ molecule to do the sensitivity analysis of splitting on cage geometry. Finally, we will explore the entanglement between the translational and rotational degrees of freedom using the measure known as the bipartite Von Neumann entanglement entropy.

4.1 The "intra-cage" Interaction is the Main Reason of Splitting

The cage geometry used in this work are obtained from combining NMR [60] and X-ray[46] in [20] and measured at 11 K where all C_{60} molecules are orientationally ordered. As is mentioned in Chapter 1, the symmetry group of solid C_{60} is $Pa\bar{3}$ such that a single C_{60} molecule has C_{3i} symmetry. The all carbons' position of a single C_{60} molecule can be determined by 10 independent carbons' coordinates since the rest of the coordinates are all C_{3i} symmetry related. The coordinates that are reported in [20] is as follows:

i	X_i	Y_i	Z_i
1	1.595	-0.540	3.123
2	0.279	-0.917	3.417
3	2.866	1.910	0.852
4	2.912	0.899	1.819
5	3.463	-0.769	0.084
6	3.215	-0.464	1.428
7	-2.831	0.277	2.121
8	-1.973	-0.510	2.907
9	-2.234	-2.402	1.353
10	-1.669	-1.864	2.516

Table 4.1: The C_{60} geometry in orientationally ordered phase given in [20].

In order to investigate the origin of the degeneracy lifting of ortho-H_2 ground state, the following situations are considered and are illustrated in Figure 4.1. The symbols used in Figure 4.1 are explained as follows: A circle stands for a C_{60} cage with Ih symmetry, a square stands for a C_{60} in the solid with C_{3i} symmetry and the two black dots connected with a solid line stands for a H_2 molecule. In a FCC lattice, one C_{60} molecule has 12 nearest neighbour cages which are illustrated by 4 squares or

4 circles for simplicity in Figure 4.1. Here, the contribution of further neighbouring C_{60} molecules is in the order of 0.01 compared to the nearest neighbour contribution. It is negligible due to the fact that L-J potential has r^{-6} decay. Moreover, the L-J interaction between H_2 and H_2 is also insignificant comparing it between H_2 and C_{60}, which justifies that no H_2 molecules was modelled inside the neighbouring C_{60} cages.

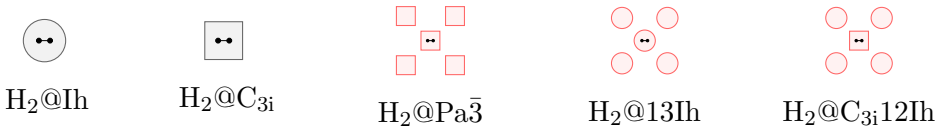

Figure 4.1: Diagrammatic representation of a H_2 sitting in different cage environments.

- H_2@13Ih: A H_2 inside a C_{60} molecule with Ih symmetry;
- H_2@C_{3i}: A H_2 inside a C_{60} molecule with C_{3i} symmetry;
- H_2@Pa$\bar{3}$: A H_2 in a C_{60} with 12 nearest neighbour C_{60} cages (Pa$\bar{3}$) in the solid state;
- H_2@13Ih: A H_2 inside a central Ih C_{60} with12 neighbouring Ih C_{60};
- H_2@C_{3i}12Ih: A H_2 inside a C_{60} with C_{3i} symmetry, with 12 neighbouring Ih C_{60} cages.

In order to investigate the role of neighbour cages, the exact diagonalizations were preformed for the above cases with all potential energy surfaces that presented in Table 2.2. The splitting (cm^{-1}) of ortho-H_2 ground state (J=1) for PES2 with H_2 in its translational ground state $\nu = 0$ were tabulated in Table 4.2. The positive splitting denotes that the three-fold J=1 state is split into a higher doubly degenerate level and a lower non-degenerate level and have the same ordering as the experimental measurements in [40]. Conversely, a negative splitting denotes that the three-fold

J=1 state is split into a higher non-degenerate level and a lower doubly degenerate level as we explained in 1.3. Similarly with the PES2, the splitting (cm^{-1}) of ortho-

	H_2@Pa$\bar{3}$	H_2@13Ih	H_2@C_{3i}12Ih	H_2@C_{3i}	H_2@Ih
p-phase	-0.1622	-0.0173	-0.1677	-0.1495	0.0000
h-phase	-0.1336	0.0157	-0.1345		

Table 4.2: The splitting of ortho-H_2(J=1) ground state for PES2ν0

H_2 ground state (J=1) for OPES with H_2 in first excited state $\nu = 1$ and in ground state $\nu = 0$ were tabulated in TABLE4.3 and TABEL4.4 respectively.

	H_2@Pa$\bar{3}$	H_2@13Ih	H_2@C_{3i}12Ih	H_2@C_{3i}	H_2@Ih
p-phase	-0.0175	-0.0020	-0.0181	-0.0160	0.0000
h-phase	-0.0141	0.0019	-0.0142		

Table 4.3: The splitting of ortho-H_2(J=1) ground state for OPESν1

	H_2@Pa$\bar{3}$	H_2@13Ih	H_2@C_{3i}12Ih	H_2@C_{3i}	H_2@Ih
p-phase	-0.0164	-0.0019	-0.0133	-0.0150	0.0000
h-phase	-0.0132	0.0018	-0.0133		

Table 4.4: The splitting of ortho-H_2(J=1) ground state for OPESν0

As we mentioned in 1.1.3, the principle that the degeneracy of otrho-H_2 ground state(J=1) is not lifted if the Ih symmetry of the C_{60} cage is maintained is confirmed by the fact that H_2@Ih gives no splitting at J=1 level for all potential energy surfaces considered. The splitting calculated on H_2 inside a distorted cage (H_2@C_{3i}) confirms that the degeneracy of otrho-H_2 ground state(J=1) is lifted if Ih symmetry is reduced to C_{3i} symmetry. The comparison between H_2 sitting in a single distorted C_{60} without (H_2@C_{3i}) and with(H_2@Pa$\bar{3}$) neighbouring cages in solid state shows that the splitting of ortho-H_2 ground state(J=1) mainly caused by the C_{60} cage

that trapped it in solid state. The fact that H_2 inside a distorted C_{60} with other distorted C_{60} as nearest neighbouring cages(H_2@Pa$\bar{3}$) or with 12 Ih C_{60} as nearest neighbouring (H_2@C_{3i}12Ih) gives almost the same splitting strongly suggests that the neighbouring cages' geometry has no crucial effects on the ortho-H_2(J=1) splitting. The p-phase and h-phase nearest neighbouring cages orientation give different values for splitting in the solid state (H_2@Pa$\bar{3}$). Whether the single cage splitting increases or decreases depends on whether it follows the same splitting ordering. For the p-phase neighbouring cages orientation, the splitting given by 12 neighbouring cages (H_2@13Ih) is negative which has the same order as with H_2 sitting in the centred single distorted C_{60} (H_2@C_{3i}) such that the size of the splitting will be increased by including the neighbouring cage (H_2@C_{3i}12Ih). For the h-phase, the splitting given by 12 neighbouring cages has opposite order with H_2 sitting in the centred single distorted C_{60} (H_2@C_{3i}) such that the magnitude of the splitting is decreased by including the neighbouring cage. The splitting is slightly different for H_2 in its vibrational ground state compared to when it is in its first excited state. In the excited state ($\nu = 1$), it has a pairing of larger bond length of H_2 molecule and smaller rotational constant. The size of the splitting is determined by the isotropic level of the potential. By adding the third term interaction between the centre of mass of H_2 and C_{60}, the potential (OPES) become more isotropic. As a result, the splitting that is given by OPES is much smaller that those given by PES2. However, the splitting is much smaller than the experimental measurements in [40] even if when consider the PES2, which suggests that the sensitivity analysis of splitting size on single cage would be the next step.

4.2 Sensitivity Analysis of Splitting on C_{60} geometry

The carbon position used in this work is from [20] and is summarized in Table 4.2. These coordinates, which are referred to as $\{\vec{R}_i^{\text{exp}}\}(i = 1...10)$ carries with experimental uncertainties which are at least in the 10^{-3}Åorder of magnitude. To

explore the possible role of the experimental uncertainties, exact diagonalizations on 40 randomly distorted cages that, nevertheless, persevere of C_{3i} symmetry were performed. These random distorted cages are formulated by adding random displacements taken from a normal distribution with a standard deviation of 0.001Å to the 10 independent coordinates $\{\vec{R}_i^{\exp}\}$ reported in [20] to get 10 independent new coordinates $\{\vec{R}_i\}$. After this,C_{3i} operators are applied onto these new coordinates to obtain a new slightly distorted cage geometry. Figure 4.2 shows how the splitting of ortho-H_2 ground state(J=1) varies from cage to cage in over 40 random distorted cages with same C_{3i} symmetry as described above for PES2 (Left) and OPES (Right) with H_2 in vibrational ground state $\nu = 0$ (red circle) or first excited state $\nu = 1$ (blue square). The splitting is slightly different for H_2 in vibra-

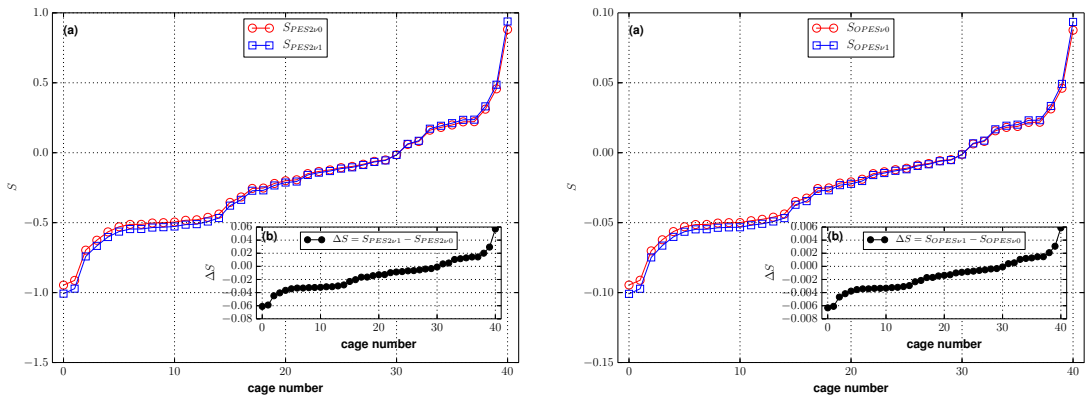

Figure 4.2: The sorted splitting (S) (cm^{-1}) varies from cage to cage in over 40 random distorted cages with C_{3i} symmetry on PES2 (Left) and OPES (Right): (a) red circle and blue square are splitting with H_2 in its vibrational ground state and first excited state. (b) The difference of splitting with H_2 in its vibrational ground state and first excited state.

tional ground state from when it was in its first excited state. This corresponds to different bond length of H_2 molecule and rotational constant, as discussed in 2.2. Higher vibrational state corresponds to smaller rotational constant,larger H_2 bond length,and larger splitting. With 0.001Å standard deviation,some geometries give

positive splitting, while some give a negative splitting. The reason that the number of cages that gives negative splitting is larger than those giving positive splitting is that start cage in [20] gives negative splitting order. This splitting extends, and is several times larger than those given by the experimental cage geometry $\{\vec{R}_{\mathrm{i}}^{\mathrm{exp}}\}$. This indicates that the splitting is extremely sensitive to the cage geometry. Given the sensitivity of splitting on the geometry,there are two perspective regarding the experimental measurements of splitting in [40]. One is that p-phase and h-phase nearest neighbouring orientation gives different splitting maybe due to fact that p-phase and h-phase neighbouring orientation may have different effect on the centred C_{60} cage geometry. The other one is that if it is possible to access the cage geometry that is used to measure splitting, one may compute comparable splitting with the experimental measurement given that for some random cages the splitting is close to the experimental measurements. Furthermore,we need to consider the quantum zero point translational motion of carbon atoms effect on the structure of C_{60} which has the magnitude of 0.044Å in [29]. This will be discussed in next chapter after an analytical approach has been developed.

4.3 Translational and Rotational Coupling

In order to explore the effects of translational and rotational coupling on the splitting of ortho-H_2 ground state (J=1), calculations using different truncated basis were preformed. The splitting calculated by exact diagonalization using a converged basis is referred to as S_{full}. The splitting calculated by exact diagonalization in converged rotational basis ($J \leq 5$) coupled with translational ground state ($n_x + n_y + n_z = 0$) is denoted as S_{ED0}. The splitting calculated by exact diagonalization in ortho-H_2 rotational ground state coupled with translational ground state is denoted as S_{PT}. The comparison of these three calculations are shown in Figure 4.3. The effect of higher rotational level ($J > 1$) coupling on J=1 splitting are negligible. The coupling between translational ground state and ortho-H_2 rotational ground state gives comparable splitting with that of those given by full calculations. To quantify the above

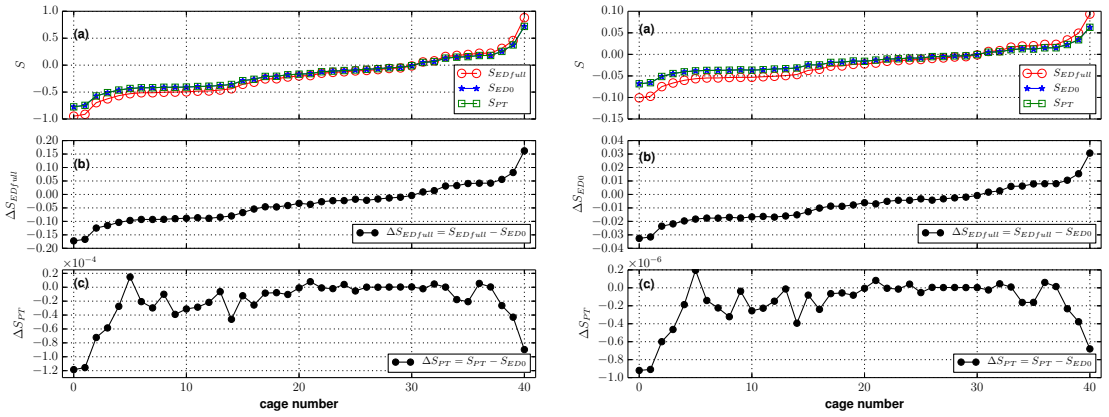

Figure 4.3: The comparison of splitting with different truncated basis on PES2ν0 (Left) and OPESν1 (Right): difference between S_{full} and S_{ED0} and difference between S_{PT} and S_{ED0}.

coupling, the entanglement between the translational and rotational degrees of freedom has been evaluated. Our measure of entanglement is known as the bipartite Von Neumann entanglement entropy:

$$S^{r}_{|\Phi\rangle} = -\operatorname{Tr}\left[\rho_r \log \rho_r\right] \quad \text{with} \quad \rho_r = \operatorname{Tr}_t |\Phi\rangle \langle\Phi| \tag{4.1}$$

In Equation 4.1, $|\Phi\rangle$ is an eigenfunction of the Hamiltonian in Equation 2.1 and ρ_r is the reduced density matrix of rotational part given by tracing out the translational part from a pure state density matrix. The results of Von Neumann entanglement entropy are showed in Table 4.5 for OPESν1 and in Table 4.6 for PES2ν0: the maximum Von Neumann entanglement entropy of the following calculation is $S_{\max}$ = log(eigenfunction size) = 7.6962. The cage geometry used in the calculation is $\{\vec{R}_i^{\exp}\}$ in [20] which gives negative splitting order. The lower doubly degenerate level have same entanglement entropy which is larger than it is for the higher non-degenerate level, as was expected. The PES2 have relative larger Von Neumann entanglement entropy than OPES, which is not predicted by the translational and rotational coupling study showing in Figure 4.3. All entanglement entropy are small comparing to the maximum. The linear combination of the basis function which

	$S^{\mathrm{r}}_{\lvert\Phi\rangle}$	Linear Combination
$\lvert\Phi=1\rangle$	0.0111	$0.344\lvert000;1\bar{1}\rangle+0.851\lvert000;11\rangle+0.206\lvert002;11\rangle+0.200\lvert020;11\rangle+0.204\lvert200;11\rangle$
$\lvert\Phi=2\rangle$	0.0111	$0.344\lvert000;11\rangle+0.851\lvert000;1\bar{1}\rangle+0.206\lvert002;1\bar{1}\rangle+0.200\lvert200;1\bar{1}\rangle+0.204\lvert020;1\bar{1}\rangle$
$\lvert\Phi=3\rangle$	0.0026	$0.917\lvert000;10\rangle+0.212\lvert002;10\rangle+0.223\lvert020;10\rangle+0.223\lvert200;10\rangle$

Table 4.5: Von Neumann entanglement entropy of ortho-H_2 state calculated using OPESν1: $|\Phi=1\rangle$ is the first eigenfunction of ortho-H_2 and the basis function is expressed in the form $|n_x n_y n_z; lm\rangle$

	$S^{\mathrm{r}}_{\lvert\Phi\rangle}$	Linear Combination
$\lvert\Phi=1\rangle$	0.0247	$0.993\lvert000;11\rangle+0.093\lvert000;1\bar{1}\rangle+0.039\lvert002;11\rangle+0.021\lvert020;11\rangle+0.024\lvert200;11\rangle$
$\lvert\Phi=2\rangle$	0.0247	$0.993\lvert000;1\bar{1}\rangle+0.093\lvert000;11\rangle+0.039\lvert002;1\bar{1}\rangle+0.021\lvert200;1\bar{1}\rangle+0.024\lvert020;1\bar{1}\rangle$
$\lvert\Phi=3\rangle$	0.0171	$0.997\lvert000;10\rangle+0.039\lvert020;10\rangle+0.039\lvert200;10\rangle$

Table 4.6: Von Neumann entanglement entropy of ortho-H_2 state calculated using PES2ν0: $|\Phi=1\rangle$ is the first eigenfunction of ortho-H_2

contributes most has been tabulated. It is showing that the basis function $|000;11\rangle$ and $|000;1\bar{1}\rangle$ are the main contributors in the lower doubly degenerate eigenstate and $|000;10\rangle$ is the main contributor to the non degenerate eigenstate. The probability amplitude of the basis $|000;10\rangle$, $|000;1\bar{1}\rangle$ and $|000;11\rangle$ in PES2 is larger than them in OPES. this may explain why the splitting calculated by exact diagonalization in converged rotational basis($J \leq 5$) coupled with translational ground state S_{ED0} recover more percentage of the splitting in PES2 than in OPES as shown by Figure 4.3.

Chapter 5

Analytical Approach

In this chapter, we will present how to solve our problem analytically by performing multipole expansion on the L-J potential. First, a very brief summary of multipole expansion on electric potential will be present which aims to give the reader a refresh of this general case. Then, we start with performing multipole expansion on L-J potential for pinned H_2 which has no translational degree of freedom comparing with that H_2 is trapped inside C_{60}. After validating the multipole expansion on L-J potential for pinned H_2, we will provide the multipole expansion on L-J potential for our real case which is H_2 trapped inside C_{60} and will be referred to unpinned case in this chapter. The formalism and validation of multipole expansion on L-J potential for unpinned H_2 will be provide, as well as the discussion of advances of this analytical approach.

5.1 A Brief Summary of Multipole Expansion for Electric Potential

As shown in Equation 2.8, the L-J potential has r^{-6} behaviours, which is similar to the Coulomb potential caused by a localized charge distribution. The Coulomb potential outside the charge distribution can be written as an expansion of spherical harmonics with properly assigned multipole moments [27]. It will be worthwhile to briefly review the formalism of the multipole expansion for Coulomb potential. Imagine that a point charge Q sitting in position $\vec{R}'(R', \Theta', \Phi')$, the Coulomb potential at position $\vec{R}(R, \Theta, \Phi)$ is given by:

$$V = \frac{Q}{|\vec{R}' - \vec{R}|}. \tag{5.1}$$

One can easily generalize this expression by simply replacing the point charge into a localized charge distribution. Assuming the localized charge distribution is described by $\rho(\vec{R}')$, the Coulomb potential can be written as follows:

$$V(\vec{R}) = \int \frac{\rho(\vec{R}')}{|\vec{R}' - \vec{R}|} d\vec{R}'. \tag{5.2}$$

If the condition $|\vec{R}| \gg |\vec{R}'|$ is satisfied, one can expand $\frac{1}{|\vec{R}' - \vec{R}|}$ into a summation of Legendre polynomials:

$$\frac{1}{|\vec{R}' - \vec{R}|} = \frac{1}{R} \sum_{l=0}^{\infty} \left(\frac{R'}{R} \right)^l P_l(\cos\gamma), \tag{5.3}$$

where $P_l(\cos\gamma)$ is the Legendre polynomials of order l and γ is the angle between $\vec{R}'$ and $\vec{R}$. The Legendre polynomials can be written as the summation of spherical harmonic functions:

$$P_l(\cos\gamma) = \frac{4\pi}{2l+1} \sum_{m=-l}^{l} Y^*_{lm}(\Theta', \Phi') Y_{lm}(\Theta, \Phi). \tag{5.4}$$

Using Equation 5.4, the Coulomb potential due to a localized charge distribution can be written as :

$$V(\vec{R}) = \sum_{lm} \frac{4\pi}{2l+1} \left[\int \rho(\vec{R}')(R')^l Y^*_{lm}(\Theta', \Phi') d\vec{R}' \right] \frac{Y_{lm}(\Theta, \Phi)}{R^{l+1}}. \tag{5.5}$$

The coefficient in the square bracket in front of $\frac{Y_{lm}(\Theta,\Phi)}{R^{l+1}}$ is known as multipole moments,

$$q_{lm} = \int \rho(\vec{R'})(R')^l Y^*_{lm}(\Theta', \Phi') d\vec{R'} \tag{5.6}$$

The coefficient q_{lm} characterizes the properties of the charge distribution density $\rho(\vec{R'})$. $l = 0$ is called the monopole term, $l = 1$ is the dipole term which relates the electric dipole moment and $l = 2$ is the quadruple term which is related to the electric quadruple moment tensor.

5.2 Multipole Expansion on L-J of Pinned H_2

5.2.1 Formalism

To start with, a hydrogen molecule assumed to be pinned at the centre of C_{60} molecule is considered since this is easier to deal with. Motivated by the multipole expansion for Coulomb potential using Legendre polynomials, the r^{-6} and r^{-12} terms of the L-J potential are expanded by using Gegenbauer polynomials. These polynomials are a generalized higher dimensional version of Legendre polynomials [3, 41]. Assuming a hydrogen atom at $\vec{r}(r, \theta, \phi)$ and i-th carbon atom at $\vec{R}_i(R_i, \Theta_i, \Phi_i)$, the $r^{-\lambda}$ term in the L-J potential can be written as follows:

$$\frac{1}{|\vec{R} - \vec{r}|^\lambda} = \frac{1}{R^\lambda} \sum_{n=0}^{\infty} \left(\frac{r^n}{R^n}\right) C_n^{\left(\frac{\lambda}{2}\right)}(\cos\gamma), \tag{5.7}$$

where $C_n^{\left(\frac{\lambda}{2}\right)}(\cos\gamma)$ are Gegenbauer polynomials and, again, γ is the angle between the $\vec{r}$ and $\vec{R}_i$. Similarly, to the Legendre polynomials, the Gegenbauer Polynomials can also be written as a summation of spherical harmonic functions by using the Addition Theorem.

$$C_n^{\lambda/2}(\cos\gamma) = \sum_{m=0}^{\lfloor n/2 \rfloor} \sum_{k=-(n-2m)}^{n-2m} \frac{4\pi}{2(n-2m)+1} B^{\lambda/2}_{n,m} Y^*_{n-2m,k}(\Theta, \Phi) Y_{n-2m,k}(\theta, \phi). \tag{5.8}$$

The $Y^*_{n-2m,k}(\Theta,\Phi)$ and $Y_{n-2m,k}(\theta,\phi)$ terms are spherical harmonics functions both with a degree of $n-2m$. B^{λ}_{nm} is a dimensionless constant and has the following form:

$$B^{\lambda/2}_{n,m} = \frac{(\lambda/2)_{n-m}\,(\lambda/2-1/2)_m\,(2n-4m+1)}{(3/2)_{n-m}m!}, \tag{5.9}$$

where $(p)_m$ is the Pochhammer symbol and more specifically it is a rising factorial. With all of the above, the multipole expansion on L-J potential of H_2 molecule pinned in the geometry centre of the C_{60} molecule can be written as:

$$V(\theta,\phi) = \sum_{l=0}^{\infty}\sum_{m=-l}^{l} Q_{lm}Y_{l,m}(\theta,\phi) \tag{5.10}$$

$$Q_{lm} = 2\sum_{k=0}^{\infty}\sum_{i=1}^{60}\frac{4\pi}{2l+1}4\epsilon\left(B^6_{l+2k,k}\frac{\sigma^{12}r^{l+2k}}{R_i^{l+2k+12}} - B^3_{l+2k,k}\frac{\sigma^6 r^{l+2k}}{R_i^{l+2k+6}}\right)Y^*_{l,m}(\Theta_i,\Phi_i). \tag{5.11}$$

The factor 2 accounts for the 2 hydrogen atoms of H_2. Similarly to the multipole moments q_{lm} of the Coulomb potential, Q_{lm} will characterize the geometry properties of C_{60} cage. A convergence study was performed in this case and, since $r \ll R$, the summation will converge very quickly. Since $k=0$ can give 75% of the real potential and $k=0,1$ gives approximately 98% of the real potential, we used $l=8$ and $k=8$ to get very accurate potentials as well as the multipole moments Q_{lm}.

5.2.2 Validation

For a H_2 molecule is pinned in the geometrical centre ofa C_{60}, only rotational degree of freedom are left to consider. The Hamiltonian only contains the rotational part and the interaction potential energy $V(\theta,\phi)$. The natural basis of this Hamiltonian is the spherical harmonic function and the matrix element has the following form:

$$\langle LM|\, H_{\text{pinned}}\, |L'M'\rangle\,. \tag{5.12}$$

In order to check the validity of the multipole expansion method, we compare the potential given by Equation 2.7 and that given by the multipole expansion expression. Here only the results for PES2 are presented since the interaction between

the centre of mass of H_2 and C_{60} cage only gives a constant shift on the potential for pinned rotor. In Figure 5.1, we show how the potential for a pinned H_2 inside

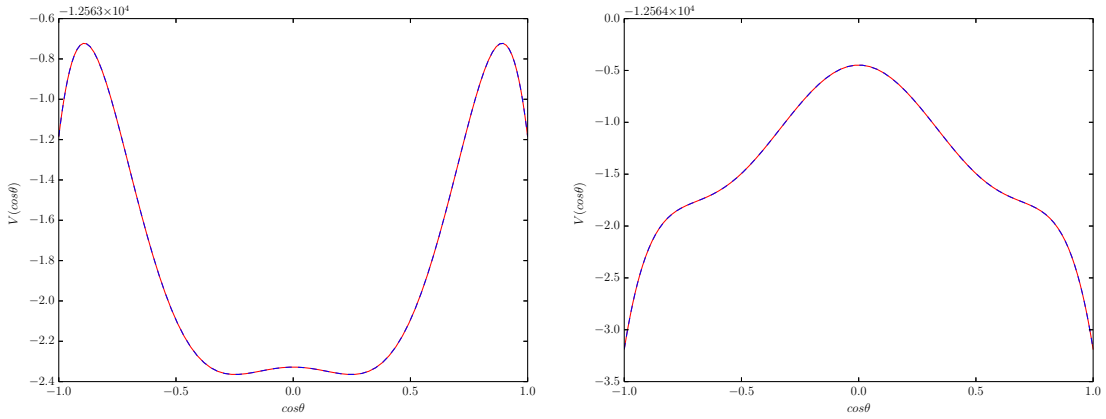

Figure 5.1: The comparison of potential dependence on $\cos\theta$ between multipole expansion (red line) and accumulation 2-site L-J potential (blue line): Left potential gives negative splitting order and right one gives positive splitting order.

C_{60} varies along different polar angle ($\cos\theta$) with averaged azimuthal angle. Our multipole expansion expression gives right results of the L-J potential for H_2 pinned at the centre of C_{60} molecule. The potential shown on the left was calculated using a cage geometry that gives negative splitting and the potential showing on the right was calculated by using another cage geometry that gives positive splitting. Due to the inversion symmetry of the cage, only even multipole term will survive in the multipole expansion, moreover by choosing z-axis along C_{3i} symmetry axis only multipole terms that has 3-fold rotational symmetry will be nonzero. The multipole term(Q_{lm}) can be tabulated in Table 5.1 for one cage geometry that gives a negative splitting and Table 5.2 for that gives positive splitting. Only results for $l \leq 6$ are showing here since higher order terms are negligible. The sign of Q_{20} is opposite since it directly related to the ortho-H_2 ground state splitting.

$$\langle 1M' | V | 1M \rangle = \int Y^*_{1M'}(\theta,\phi) Q_{20} Y_{20}(\theta,\phi) Y_{1,M}(\theta,\phi) \sin\theta d\theta d\phi. \tag{5.13}$$

Furthermore,the comparison between analytical approach and numerical calcula-

	l=2	l=4	l=6
m=-6			0.085+0.021i
m=-3		0.027-0.031i	0.137+0.017i
m=0	0.336	-0.029	-0.091
m=3		-0.027-0.031i	-0.137+0.017i
m=6			0.085-0.021i

Table 5.1: The tabulation of multipole term(Q_{lm}) with PES2 that gives negative splitting

	l=2	l=4	l=6
m=-6			0.088+0.021i
m=-3		0.086+0.013i	0.136+0.018i
m=0	-0.356	0.042	-0.091
m=3		-0.086+0.013i	-0.136+0.018i
m=6			0.088-0.021i

Table 5.2: The tabulation of multipole term(Q_{lm}) with PES2 that gives positive splitting

tion are showing in Figure 5.2 for PES2ν0. The S_{EDfull} is the splitting calculated by exact diagonalization under converged basis. The S_{PT} is the splitting calculated by exact diagonalization in ortho-H_2 ground state (J=1), which is the first order degeneracy perturbation theory given by $\langle 1M'|\, V\, |1M\rangle$. The $S_{multipole}$ is the splitting calculated by multipole expansion by using Equation 5.13. The agreement of numerical calculation and analytical multipole expansion calculation adjusted by the insert figure(c) in Figure 5.2 and the error is in the order of 10^{-8}. Similar with unpinned case, the higher rotational state coupling is negligible given that

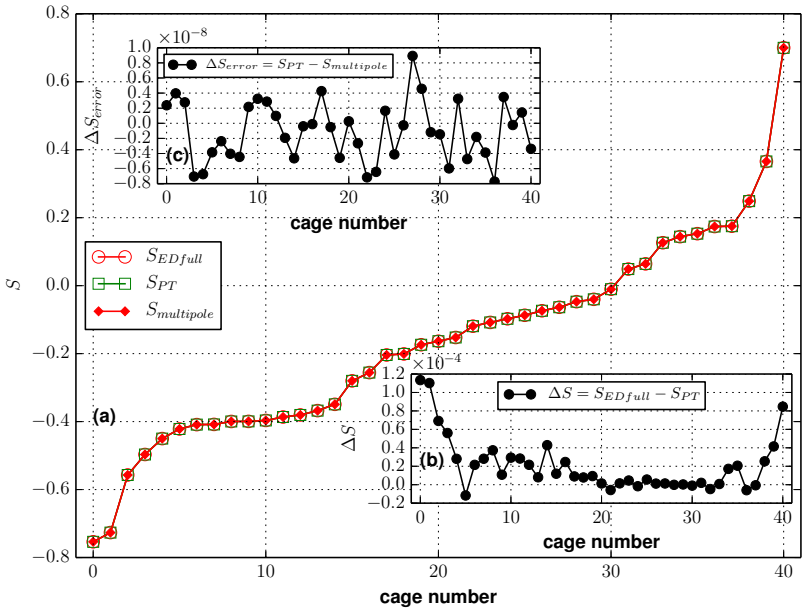

Figure 5.2: The comparison between analytical approach and numerical calculation for pinned rotor with PES2: The S_{PT} is the splitting calculated by exact diagonalization in ortho-H_2 ground state(J=1), which is the first order degeneracy perturbation theory given by $\langle 1M'|\, V\, |1M\rangle$. The $S_{multipole}$ is the splitting calculated by multipole expansion by using Equation 5.13.

the difference between full calculation and perturbation is in the order of 10^{-4} as show in insert figure(b) in Figure 5.2. The same calculation was also conducted for OPES and it shows same qualitative behaviours which can be found in appendix. For pinned rotor, It shows that the numerical exact diagonalization agrees with the analytical approach and the splitting of ortho-H_2 ground state can be computed by using dipolar term Q_{20} with very small error. The splitting order will determined by the sign of the dipolar term Q_{20} which reflects the geometry feature of the C_{60} cages. after solving the above problems for pinned case, It is time to move onto our real topic that H_2 confined inside C_{60}, which also referred as unpinned H_2.

5.3 Multipole Expansion on L-J of Unpinned H_2

5.3.1 Formalism

Having developed the formation for the multipole expansion for the case that a H_2 molecule pinned at the geometry centre of C_{60} which only have rotational degree of freedom. We can now consider H_2 with its five dimensional degrees of freedom, which are characterized by centre of mass motion $\vec{\delta}(\delta, \theta_\delta, \phi_\delta)$ and $\vec{r}(r, \theta, \phi)$. $\vec{r}$ specify the orientation of H_2 respect to center of mass where r is half of the bond length of H_2. $\vec{\delta}$ specify the position of the center of mass of H_2. We use $\vec{R_i}(R_i, \Theta_i, \Phi_i)$ to specify the position of i-th carbon atom from the origin. We have the following vector relation:

$$\vec{d_{1i}} = \vec{R_i} - \vec{\delta} - \vec{r},$$
$$\vec{d_{2i}} = \vec{R_i} - \vec{\delta} + \vec{r},$$

where $\vec{d_{1i}}$ and $\vec{d_{2i}}$ refer to the vector from hydrogen atom 1 and hydrogen atom 2 to i-th carbon atom. The main difficulties of moving from a description of pinned H_2 inside C_{60} to the unpinned H_2 inside C_{60} is to deal with the translational degrees of freedom. Suggested by the numerical work in 4.3 that the coupling between translational ground state and ortho-H2 rotational ground state gives comparable splitting with that of those given by full calculations, we can assume that the centre of mass motion can be described by the ground state of isotropic harmonic oscillator which has the following form:

$$\psi_{nlm}(r, \theta, \phi) = R_{nl}(r) Y_{lm}(\theta, \phi) \quad \text{with} \int_0^\infty |R_{nl}(r)|^2 r^2 dr = 1.$$

The centre of mass of H_2 in the ground state have the following form:

$$\psi_{000}(\delta, \theta_\delta, \phi_\delta) = R_{00}(\delta) Y_{00}(\theta_\delta, \phi_\delta) = \left(\frac{2\nu^3}{\pi}\right)^{\frac{1}{4}} \sqrt{8} \exp\{-\nu\delta^2\} \frac{1}{\sqrt{4\pi}}, \tag{5.14}$$

where ν is defined as $\nu = \frac{\mu\omega}{2\hbar}$, μ is the mass of H_2 and ω is the angular frequency of the oscillator. We can now perform a multipole expansion of an unpinned rotor with

centre of mass in translational ground state. Firstly, the potential can be written as following given that H_2 is the translational ground state:

$$\langle 000|\,\hat{V}\,|000\rangle = \int_0^{\infty}\int_{-1}^{1}\int_0^{2\pi} |R_{00}(\delta)|^2\,\delta^2 |Y_{00}(\theta_\delta,\phi_\delta)|^2 V(|\vec{R_i}-\vec{r}-\vec{\delta}|)d\delta\; d\cos\theta_\delta\; d\phi_\delta. \tag{5.15}$$

Similar with the pinned rotor case, we treated $\vec{R_i}-\vec{r}$ together and expand the potential in terms of $\vec{\delta}$ since the condition $|\vec{\delta}| \ll |\vec{R_i}-\vec{r}|$ holds in this case. we got the following:

$$V(\delta,\theta_\delta,\phi_\delta) = \sum_{l,m}\sum_{k=0}^{\infty}\sum_{i=1}^{60}\frac{4\pi}{2l+1}\left(\frac{4\epsilon\sigma^{12}B^6_{l+2k,k}\delta^{l+2k}}{|\vec{R_i}-\vec{r}|^{l+2k+12}} - \frac{4\epsilon\sigma^{6}B^3_{l+2k,k}\delta^{l+2k}}{|\vec{R_i}-\vec{r}|^{l+2k+6}}\right) Y^*_{lm}(\widehat{\vec{R_i}-\vec{r}})Y_{lm}(\theta_\delta,\phi_\delta), \tag{5.16}$$

where $\widehat{\vec{R_i}-\vec{r}}$ means the angle of vector $\vec{R_i}-\vec{r}$. Now, we can plug Equation 5.16 into Equation 5.15. We use the following properties of the spherical harmonic function:

$$\frac{1}{\sqrt{4\pi}}\int_{-1}^{1}\int_0^{2\pi} Y_{nm}(\theta,\phi)d\cos(\theta)d\phi = \delta_{n,0}\delta_{m,0}, \tag{5.17}$$

where $\delta_{n,0}\delta_{m,0}$ are Kronecker delta function. This allow to simplify the expansion significantly since only the $l=0$ and $m=0$ terms survived. The Equation 5.15 can be rewritten as following:

$$\langle 000|\,\hat{V}\,|000\rangle = \int_0^{\infty}|R_{00}(\delta)|^2\,\delta^2\sum_{k=0}^{\infty}\sum_{i=1}^{60}\left(\frac{4\epsilon\sigma^{12}B^6_{2k,k}\delta^{2k}}{|\vec{R_i}-\vec{r}|^{2k+12}} - \frac{4\epsilon\sigma^{6}B^3_{2k,k}\delta^{2k}}{|\vec{R_i}-\vec{r}|^{2k+6}}\right)d\delta. \tag{5.18}$$

Then, one find that Equation 5.18 can be further expanded again with respect to $\vec{r}$ by using Equation5.7 and Equation5.8. Now we use prime for each label:

$$\frac{1}{|\vec{R_i}-\vec{r}|^{2k+12}} = \frac{1}{|\vec{R_i}|^{2k+12}}\sum_{l',m'}\sum_{k'=0}^{\infty}\frac{4\pi}{2l'+1}B^{k+6}_{l'+2k',k'}\frac{|\vec{r}|^{l'+2k'}}{|\vec{R_i}|^{l'+2k'}}Y^*_{l'm'}(\Theta_i,\Phi_i)Y_{l'm'}(\theta,\phi) \tag{5.19}$$

Then the Equation 5.18 can be written as following:

$$\langle 000|\,\hat{V}\,|000\rangle = \sum_{l=0}^{\infty}\sum_{m=-l}^{m=l}A_{lm}Y_{lm}(\theta,\phi) \tag{5.20}$$

with $A_{l'm'}$ has the following form and for simplicity only the repulsive part of L-J potential are presented here and we can obtain the attractive term by replacing 12 by 6 and 6 by 3:

$$A_{l'm'} = \sum_{k,k'=0}^{\infty} \sum_{i=1}^{60} \int_0^{\infty} |R_{00}(\delta)|^2 \, \delta^{2+2k} d\delta \frac{4\pi}{2l'+1} 4\epsilon \left(\frac{\sigma^{12} B_{2k,k}^6 B_{l'+2k',k'}^{k+6} |\vec{r}|^{l'+2k'}}{|\vec{R}_i|^{l'+2k'+2k+12}} \right) Y_{l'm'}^*(\Theta_i, \Phi_i) \tag{5.21}$$

The coefficient $A_{l'm'}$ is an analogue of Q_{lm} which we defined for pinned rotor before. Again the factor of 2 is still needed to count in two hydrogen atoms by symmetry. Now it is time to evaluate the integral of the translational part:

$$\int_0^{\infty} |R_{00}(\delta)|^2 \, \delta^{2+2k} d\delta = 8\nu \frac{(2k+1)!!}{2^{k+2}(2\nu)^{k+1}}, \tag{5.22}$$

according to the following handy integral rules:

$$\int_0^{\infty} x^{2n} \exp\{-ax^2\} dx = \frac{(2n-1)!!}{2^{n+1} a^n} \left(\frac{\pi}{a}\right)^{1/2}.$$

We can now put everything together to get final result for the repulsive term of the L-J potential of the interaction between one hydrogen atom and the i-th carbon atom:

$$A_{lm} = \sum_{k,k'=0}^{\infty} \frac{8\nu(2k+1)!!}{2^{k+2}(2\nu)^{k+1}} \frac{4\pi |\vec{r}|^{l+2k'}}{2l+1} \frac{4\epsilon\sigma^{12} B_{2k,k}^6 B_{l+2k',k'}^{k+6}}{|\vec{R}_i|^{l+2k'+2k+12}} Y_{lm}^*(\Theta_i, \Phi_i) \tag{5.23}$$

Now the value of ortho-H_2 rotational ground state block(J=1) are easy to evaluate, since only $l' = 2$ term give nonzero value according to the properties of Clebsch-Gordan coefficients. Moreover, if the z-axis is align along the C_{3i} symmetry axis, only $m' = 0$ term will be nonzero by the space group argument.

$$\langle 1M' | \langle 000 | V | 000 \rangle | 1M \rangle = \int Y_{1M'}^*(\theta, \phi) A_{20} Y_{20}(\theta, \phi) Y_{1,M}(\theta, \phi) \sin\theta d\theta d\phi. \tag{5.24}$$

Above is the multipole expansion for unpinned H_2 molecule confined into C_{60} molecule with the assumption that H_2 is in translational ground state. We can justify our analytical result by comparing with block diagonalization calculation. For OPES,the

interaction potential between the centre of mass of H_2 and C_{60} can be expand as following which is directly took from Equation5.18 with $\vec{r} = 0$ and integrate over translational radius part:

$$\langle 000| V(|\vec{R}_i - \vec{\delta}|) |000\rangle = \sum_{k=0}^{\infty} \sum_{i=1}^{60} 8\nu \frac{(2k+1)!!}{2^{k+2}(2\nu)^{k+1}} \left(\frac{4\epsilon\sigma^{12} B^6_{2k,k}}{|\vec{R}_i|^{2k+12}} - \frac{4\epsilon\sigma^6 B^3_{2k,k}}{|\vec{R}_i|^{2k+6}} \right) \quad (5.25)$$

This term is a constant and it will not lift the degeneracy or cause splitting under the assumption that H_2 is in translational ground state. This argument can also be justified by comparing analytical result and block diagonalization calculation with the OPES potential.

5.3.2 Validation

The L-J potential has been expanded as a summation of spherical harmonics functions under the assumption that H_2 is in its translational ground state. The potential calculated by multipole expansion with Equation 5.20 and Equation 5.21 is compared with it calculated by accumulated 2-site or 3-site L-J potential. The potential of PES2ν0 is shown in Figure 5.3. Again, similarly with pinned case, the left

	l=2	l=4	l=6
m=-6			0.118+0.029i
m=-3		0.039-0.044i	0.191+0.024i
m=0	0.495	-0.042	0.126
m=3		-0.039-0.044i	-0.091+0.024i
m=6			0.118-0.029i

Table 5.3: The tabulation of multipole term(A_{lm}) with PES2ν0 that gives negative splitting.

potential is from a cage that gives negative splitting order and the right one is from a cage that gives positive splitting order. The multipole terms that gives the above

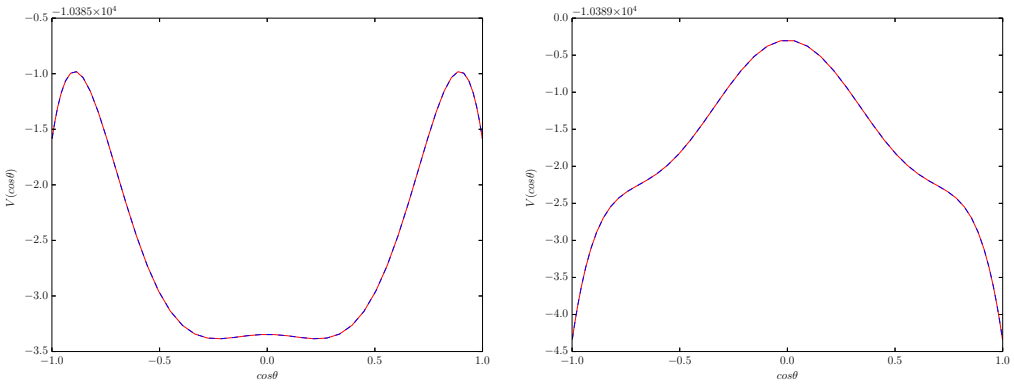

Figure 5.3: The comparison of potential dependence on $\cos\theta$ between multipole expansion (red line) and L-J potential (blue line) for unpinned H_2 with PES2ν0: Left potential gives negative splitting order and right one gives positive splitting order.

PES2 potential are tabulated in Table 5.3 for negative splitting and Table 5.4 for positive splitting. The validation of the multipole expansion can simply be justi-

	l=2	l=4	l=6
m=-6			0.123+0.030i
m=-3		0.123+0.019i	0.189+0.024i
m=0	-0.538	0.060	-0.126
m=3		0.123-0.019i	-0.189+0.024i
m=6			0.123-0.030i

Table 5.4: The tabulation of multipole term(A_{lm}) with PES2ν1that gives positive splitting

fied by the comparison of splitting that calculated numerically and analytically as shown in Figure 5.4. The multipole expansion calculation that given by Equation 5.24 agrees with the block diagonal. The error is of the order of 10^{-9} as showing in

the insert figure(b) in Figure 5.4.

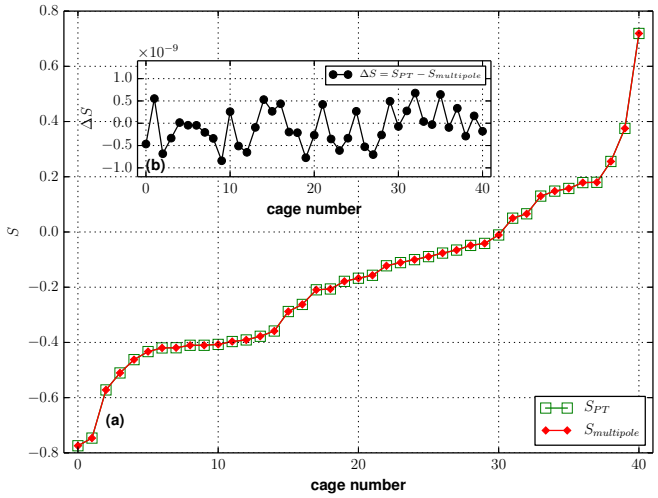

Figure 5.4: The comparison of block diagonalization calculation and multipole expansion calculation on PES2ν0.

For OPES, the interaction potential between the centre of mass of H_2 and C_{60} can be expand as following which is directly took from Equation 5.18 with $\vec{r} = 0$ and integrate over translational radius part. This term is a constant and it will not lift the degeneracy or cause splitting under the assumption that H_2 is in translational ground state. The comparison in Figure 5.5 of potential calculated by multipole expansion with Equation 5.20 and Equation 5.21 is compared with it calculated by OPES but without the interaction between centre of mass of H_2 and C_{60} cage. The multiple moments for OPESν1 that give the above potential can be found in Table 5.5 for negative splitting order and in Table5.6 for positive splitting order. The validation of the multipole expansion can simply be justified by the comparison of splitting that calculated numerically and analytically as shown in Figure 5.6. The fact the interaction between the centre of mass of H_2 and the cage does not affect the ortho-H_2 ground state splitting under the assumption that H_2 is in its translational ground

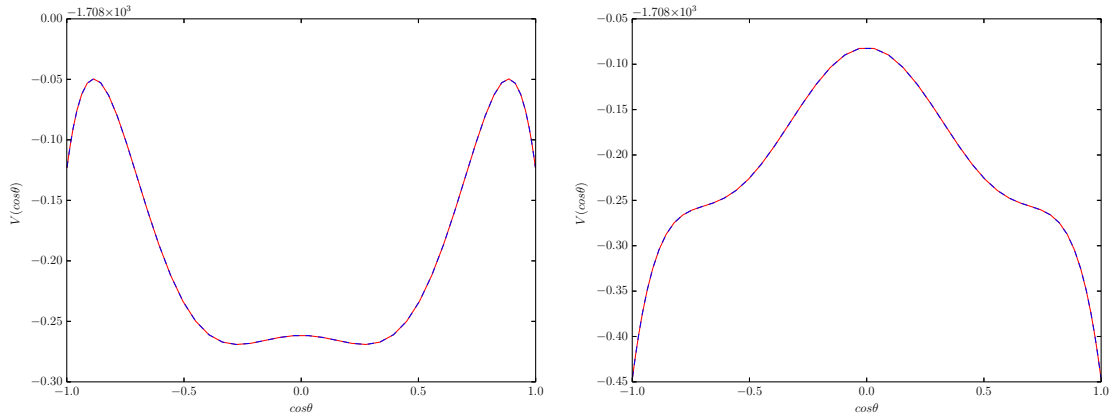

Figure 5.5: The comparison of potential dependence on $\cos\theta$ between multipole expansion (red line) and L-J potential (blue line) for unpinned H_2 with OPESν1: Left potential gives negative splitting order and right one gives positive splitting order.

	l=2	l=4	l=6
m=-6			0.013+0.003i
m=-3		0.004-0.004i	0.020+0.003i
m=0	0.044	-0.004	-0.013
m=3		-0.004-0.004i	-0.020+0.003i
m=6			0.013-0.003i

Table 5.5: The tabulation of multipole term (A_{lm}) with OPESν1 that gives negative splitting

state was therefore justified. For the unpinned rotor, the multipole expansion on L-J potential have been developed under the assumption that H_2 in its translational ground state. The analytical approach agrees with numerical results very well and the multipole moments can predict the splitting order. It also provides us a more

	l=2	l=4	l=6
m=-6			0.013+0.003i
m=-3		0.012+0.002i	0.020+0.003i
m=0	-0.046	0.006	-0.013
m=3		-0.012+0.002i	-0.020+0.003i
m=6			0.013-0.003i

Table 5.6: The tabulation of multipole term (A_{lm}) with OPESν1 that gives negative splitting.

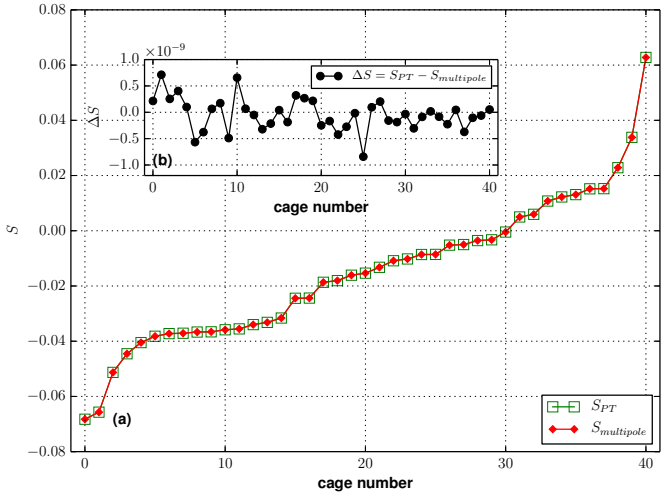

Figure 5.6: The comparison of block diagonalization calculation and multipole expansion calculation on OPESν1.

efficient way to calculate the splitting compared to the exact diagonalization method.

Chapter 6

Conclusion

6.1 Conclusion of Present Work

In this work we have discussed the subject of confined quantum molecular degrees of freedom when a small molecule H_2 is confined inside C_{60} fullerene molecule. We used the simplest possible Hamiltonian composed of translational term, rotational term and interaction term to encapsulate the quantum dynamics of the confined H_2 molecule. The interaction term can be effectively handled with L-J potential which is a simple model that approximates the interaction between H_2 and C_{60}. The method we used to deal with this problem is exact diagonalization. A variety of L-J potential parameters according to experimental measurements were used to obtain the energy levels of the trapped H_2. The reason for the splitting of ortho-H_2 ground state (J=1) has been identified to be because of the reduction from Ih symmetry to C_{3i} symmetry, which is reflected by the interaction between H_2 and its C_{60} cage instead of that between $H_2@C_{60}$ with its neighbouring molecules. The fact that ortho-H_2 ground sate(J=1) does not split if the Ih symmetry is maintained has been justified. The reason for the splitting of ortho-H_2 ground state(J=1) has been identified to be because of the reduction from Ih symmetry to C_{3i} symmetry. It is mainly caused by the interaction between H_2 and its C_{60} cage instead of that between $H_2@C_{60}$ with its neighbouring molecules. We also found that the splitting is extremely sensitive to its

cage geometry while sitting in a relatively large linear regime. This feature suggests that the zero point motion of carbon atoms would not effect the size of the splitting. These behaviour are independent of L-J potential parameters as we expected. We also found an analytical approach to solve our problem which is doing multipole expansion on L-J potential. This analytical approach was preformed basing on the fact that the coupled motion of translational ground state and rotational ortho-ceH2 ground state(J=1) gives comparable splitting with that given by converged basis. This analytical approach gives physical understanding of energy degeneracy from symmetry perspective. We further verified that the analytical results agrees with that calculated from exact diagonalization.

Finally, a discussion of future work left for studying confined molecular degree of freedom will be present. For $H_2@C_{60}$, a more precise potential to better describe the interaction between H_2 and C_{60} would be more sufficient to study the quantum dynamics of confined H_2 molecule. A more precise potential provide us a more accurate model to confirm the above conclusions. From the study of $H_2@C_{60}$, we can extend our study into other endofullerene, such as $H_2O@C_{60}$ and $HF@C_{60}$. Comparing with $H_2@C_{60}$, the only difference is that the confined molecule H_2O and HF are dipolar molecule and will involve the long range dipole-dipole interaction.

6.2 Future Directions

6.2.1 More Precise Potential

We begun this subsection with a discussion for obtaining more precise potential to physically describe H_2 trapped inside C_{60}. Instead of parametrizing L-J potential with the experimentally measured energy level, there exists another potential to characterize this interaction. It involves writing the potential into a series of spherical harmonics physically based on the symmetry of the system and fitting into IR spectra to obtain the coefficients of the spherical harmonics [17, 45]. However, to deal with this problem, this potential will not be sufficient due to the fact that the

splitting of ortho-H_2 ground state(J=1) is small and can not be measured accurately. Therefore, fitting with IR spectra to parametrize L-J potential is the only way for now to study the degeneracy lifting of ortho-H_2 ground state(J=1). An additional direction of future work is that instead of fitting into IR spectra one can preform Ab-initio calculation to obtain coefficients of the spherical harmonics with high accuracy.

6.2.2 Dipolar Molecule Confined Inside C_{60}

In this subsection, we will describe another potential future direction of this work. The simplest possible Hamiltonian will have one more term which is the dipolar interaction term and have the following form:

$$H_{\text{dipole-dipole}} = \frac{\mu^2}{4\pi\epsilon r_{\text{nn}}^3} \sum_{i>j} \frac{\hat{n}_i \hat{n}_j - 3\hat{n}_i \cdot \hat{r}_{ij} \hat{r}_{ij} \cdot \hat{n}_j}{(r_{ij}/r_{\text{nn}})^3}. \tag{6.1}$$

In Equation 6.1, μ is the dipole moment of $H_2O@C_{60}$ or $HF@C_{60}$ and pointing in $\hat{n}_i$ direction. $\hat{r}_{ij}$ is the unit vector pointing from i-th dipole to j-th dipole with distance r_{ij} and r_{nn} is the nearest neighbour distance of $H_2O@C_{60}$ or $HF@C_{60}$ lattice. Of equal interest experimentally and theoretically, dipolar molecule confined inside C_{60}, such as H_2O and HF, could result in a net polarization due to the very long-range dipolar interactions. The periodic lattices of endofullerene complexes with polar molecules trapped inside the C_{60} can, theoretically, exhibit ferroelectric phase transition as predicted in [9]. While experimentalists did not observe any ferroelectric phase transition [1, 31]. More theoretical efforts are needed in order to predict the collective orientation of dipolar molecule and phase transition diagrams for endofullerene complexes with polar molecules trapped inside.

References

[1] Shinobu Aoyagi, et al. *Chemical Communications*, 50(5):524–526, 2014.

[2] T Atake, T Tanaka, H Kawaji, K Kikuchi, K Saito, S Suzuki, I Ikemoto, and Y Achiba. Heat capacity measurements and thermodynamic studies of the new compound c60. *Physica C: Superconductivity*, 185:427–428, 1991.

[3] John S Avery. *Hyperspherical harmonics: applications in quantum theory*, volume 5. Springer Science & Business Media, 2012.

[4] WP Beyermann, MF Hundley, JD Thompson, FN Diederich, and G Grüner. Low-temperature specific heat of c 60. *Physical review letters*, 68(13):2046, 1992.

[5] V Buntar, HW Weber, and M Ricco. Magnetic irreversibility of c60, c70 and i? c60 fullerenes at low temperature: Transition to a frozen magnetic glass state? *Solid state communications*, 98(2):175–178, 1996.

[6] M Carravetta, A Danquigny, S Mamone, F Cuda, OG Johannessen, I Heinmaa, K Panesar, R Stern, MC Grossel, AJ Horsewill, et al. Solid-state nmr of endohedral hydrogen–fullerene complexes. *Physical Chemistry Chemical Physics*, 9(35):4879–4894, 2007.

[7] Yan Chai, Ting Guo, Changming Jin, Robert E Haufler, LP Felipe Chibante, Jan Fure, Lihong Wang, J Michael Alford, and Richard E Smalley. Fullerenes with metals inside. *The Journal of Physical Chemistry*, 95(20):7564–7568, 1991.

[8] Judy Y-C Chen, Yongjun Li, Michael Frunzi, Xuegong Lei, Yasujiro Murata, Ronald G Lawler, and Nicholas J Turro. Nuclear spin isomers of guest molecules in h2@ c60, h2o@ c60 and other endofullerenes. *Phil. Trans. R. Soc. A*, 371(1998):20110628, 2013.

[9] Jerzy Cioslowski and Asiri Nanayakkara. Endohedral fullerites: a new class of ferroelectric materials. *Physical review letters*, 69(19):2871, 1992.

[10] WIF David, RM Ibberson, and T Matsuo. High resolution neutron powder diffraction: A case study of the structure of c _{60}. In *Proceedings of the Royal Society of London A: Mathematical, Physical and Engineering Sciences*, volume 442, pages 129–146. The Royal Society, 1993.

[11] Zheng-Hong Dong, Ping Zhou, JM Holden, PC Eklund, MS Dresselhaus, and G Dresselhaus. Observation of higher-order raman modes in c 60 films. *Physical Review B*, 48(4):2862, 1993.

[12] Mildred S Dresselhaus, Gene Dresselhaus, and Peter C Eklund. *Science of fullerenes and carbon nanotubes: their properties and applications*. Academic press, 1996.

[13] Mildred S Dresselhaus, Gene Dresselhaus, and Ado Jorio. *Group theory: application to the physics of condensed matter*. Springer Science & Business Media, 2007.

[14] Peter M Felker and Zlatko Bačić. Translation-rotation states of h2 in c60: New insights from a perturbation-theory treatment. *The Journal of Chemical Physics*, 145(8):084310, 2016.

[15] RM Fleming, Av P Ramirez, MJ Rosseinsky, DW Murphy, RC Haddon, SM Zahurak, and AV Makhija. Relation of structure and superconducting transition temperatures in a3c60. *Nature*, 352(6338):787–788, 1991.

[16] Lorenzo Fortunato and Francisco Pérez-Bernal. Algebraic theory of endohedrally confined diatomic molecules: Application to h 2@ c 60. *Physical Review A*, 94(3):032508, 2016.

[17] Min Ge, U Nagel, D Hüvonen, T Rõõm, S Mamone, MH Levitt, M Carravetta, Y Murata, K Komatsu, JY-C Chen, et al. Interaction potential and infrared absorption of endohedral h2 in c60. *The Journal of chemical physics*, 134(5):054507, 2011.

[18] E Grivei, B Nysten, M Cassart, A Demain, and JP Issi. Specific heat of fullerenes extract. *Solid state communications*, 85(2):73–75, 1993.

[19] RC Haddon, Louis E Brus, and Krishnan Raghavachari. Electronic structure and bonding in icosahedral c60. *Chemical Physics Letters*, 125(5-6):459–464, 1986.

[20] A Brooks Harris and Ravi Sachidanandam. Orientational ordering of icosahedra in solid c 60. *Physical Review B*, 46(8):4944, 1992.

[21] Paul A Heiney, Gavin BM Vaughan, John E Fischer, Nicole Coustel, David E Cox, John RD Copley, DA Neumann, WA Kamitakahara, Kathleen M Creegan, Donald M Cox, et al. Discontinuous volume change at the orientational-ordering transition in solid c 60. *Physical Review B*, 45(8):4544, 1992.

[22] S Hoen, NG Chopra, X-D Xiang, R Mostovoy, Jianguo Hou, WA Vareka, and A Zettl. Elastic properties of a van der waals solid: C 60. *Physical Review B*, 46(19):12737, 1992.

[23] AJ Horsewill, K Goh, S Rols, J Ollivier, MR Johnson, MH Levitt, M Carravetta, S Mamone, Y Murata, JY-C Chen, et al. Quantum rotation and translation of hydrogen molecules encapsulated inside c60: temperature dependence of inelastic neutron scattering spectra. *Philosophical Transactions of the Royal Society of London A: Mathematical, Physical and Engineering Sciences*, 371(1998):20110627, 2013.

[24] AJ Horsewill, KS Panesar, S Rols, J Ollivier, MR Johnson, M Carravetta, S Mamone, MH Levitt, Y Murata, K Komatsu, et al. Inelastic neutron scattering investigations of the quantum molecular dynamics of a h 2 molecule entrapped inside a fullerene cage. *Physical Review B*, 85(20):205440, 2012.

[25] AJ Horsewill, S Rols, MR Johnson, Y Murata, M Murata, K Komatsu, M Carravetta, S Mamone, MH Levitt, JY-C Chen, et al. Inelastic neutron scattering of a quantum translator-rotator encapsulated in a closed fullerene cage: Isotope effects and translation-rotation coupling in h 2@ c 60 and hd@ c 60. *Physical Review B*, 82(8):081410, 2010.

[26] Y Iwasa and T Takenobu. Superconductivity, mott–hubbard states, and molecular orbital order in intercalated fullerides. *Journal of Physics: Condensed Matter*, 15(13):R495, 2003.

[27] J David Jackson. *Electrodynamics*. Wiley Online Library, 1975.

[28] Satoshi Kaneko, Yoshifumi Hashikawa, Shintaro Fujii, Yasujiro Murata, and Manabu Kiguchi. Single molecular junction study on h2o@ c60: H2o is ?electrostatically isolated? *ChemPhysChem*, 18(10):1229–1233, 2017.

[29] Jorge Kohanoff, Wanda Andreoni, and Michele Parrinello. Zero-point-motion effects on the structure of c 60. *Physical Review B*, 46(7):4371, 1992.

[30] Koichi Komatsu, Michihisa Murata, and Yasujiro Murata. Encapsulation of molecular hydrogen in fullerene c60 by organic synthesis. *Science*, 307(5707):238–240, 2005.

[31] Andrea Krachmalnicoff, Richard Bounds, Salvatore Mamone, Shamim Alom, Maria Concistrè, Benno Meier, Karel Kouřil, Mark E Light, Mark R Johnson, Stéphane Rols, et al. The dipolar endofullerene hf@ c60. *Nature chemistry*, 8(10):953–957, 2016.

[32] Frederik C Krebs and Kion Norrman. Analysis of the failure mechanism for a stable organic photovoltaic during 10 000 h of testing. *Progress in Photovoltaics: Research and Applications*, 15(8):697–712, 2007.

[33] Harold Kroto. Space, stars, c 60, and soot. *Science*, 242(4882):1139–1145, 1988.

[34] Harold W Kroto, James R Heath, Sean C O'Brien, Robert F Curl, and Richard E Smalley. C60: Buckminsterfullerene. *Nature*, 318(6042):162–163, 1985.

[35] Kei Kurotobi and Yasujiro Murata. A single molecule of water encapsulated in fullerene c60. *Science*, 333(6042):613–616, 2011.

[36] Malcolm H Levitt and Anthony J Horsewill. Nanolaboratories: physics and chemistry of small-molecule endofullerenes, 2013.

[37] Tun Lu, Evelyn M Goldfield, and Stephen K Gray. Quantum states of hydrogen and its isotopes confined in single-walled carbon nanotubes: Dependence on interaction potential and extreme two-dimensional confinement. *The Journal of Physical Chemistry B*, 110(4):1742–1751, 2006.

[38] S Mamone, Min Ge, D Hüvonen, U Nagel, A Danquigny, F Cuda, MC Grossel, Y Murata, K Komatsu, MH Levitt, et al. Rotor in a cage: Infrared spectroscopy of an endohedral hydrogen-fullerene complex, 2009.

[39] Salvatore Mamone, et al. *Coordination Chemistry Reviews*, 255(7):938–948, 2011.

[40] Salvatore Mamone, Mark R Johnson, Jacques Ollivier, Stéphane Rols, Malcolm H Levitt, and Anthony J Horsewill. Symmetry-breaking in the h 2@ c 60 endofullerene revealed by inelastic neutron scattering at low temperature. *Physical Chemistry Chemical Physics*, 18(3):1998–2005, 2016.

[41] Claus Müller. *Analysis of spherical symmetries in Euclidean spaces*, volume 129. Springer Science & Business Media, 2012.

[42] Takeo Oku. Hydrogen storage in boron nitride and carbon nanomaterials. *Energies*, 8(1):319–337, 2014.

[43] EK Parks, L Zhu, J Ho, and SJ Riley. The structure of small nickel clusters. i. ni3–ni15. *The Journal of chemical physics*, 100(10):7206–7222, 1994.

[44] Frank Rioux. Quantum mechanics, group theory, and c (60). *Journal of chemical education*, 71(6):464, 1994.

[45] T Rõõm, L Peedu, Min Ge, D Hüvonen, U Nagel, Shufeng Ye, Minzhong Xu, Z Bačić, S Mamone, MH Levitt, et al. Infrared spectroscopy of small-molecule endofullerenes. *Phil. Trans. R. Soc. A*, 371(1998):20110631, 2013.

[46] Ravi Sachidanandam and A Brooks Harris. Comment on ??orientational ordering transition in solid c 60?? *Physical review letters*, 67(11):1467, 1991.

[47] Kiyoshi Sakaue, Naoki Toyoda, Hirofumi Kasatani, Hikaru Terauchi, Takeshi Arai, Youichi Murakami, and Hiroyoshi Suematsu. X-ray study of glassy behavior in c60 single crystals. *Journal of the Physical Society of Japan*, 63(4):1237–1240, 1994.

[48] Hisanori Shinohara and Nikos Tagmatarchis. *Endohedral metallofullerenes: Fullerenes with metal inside*. John Wiley & Sons, 2015.

[49] Kasthuri Srinivasan, Hemant Mahawar, and Vivek Sarin. A multipole based treecode using spherical harmonics for potentials of the form r-lˆ\ rm-\ it λ. *Computational Science–ICCS 2005*, pages 107–114, 2005.

[50] Peter W Stephens, Laszlo Mi1a1y, Peter L Lee, Robert L Whetteni, Shiou-Mei Huangi, Richard Kaneri, and Francois Deiderfchi. Structure of single-phase superconducting k36 ? *Physics & Chemistry of Fullerenes: A Reprint Collection*, 1:134, 1993.

[51] Gavin BM Vaughan, Paul A Heiney, David E Cox, Andrew R McGhie, David R Jones, Robert M Strongin, Maria A Cichy, and Amos B Smith. The orienta-

tional phase transition in solid buckminsterfullerene epoxide (c60o). *Chemical physics*, 168(1):185–193, 1992.

[52] JH Weaver, José Luís Martins, Tr Komeda, Y Chen, TR Ohno, GH Kroll, N Troullier, RE Haufler, and RE Smalley. Electronic structure of solid c 60: Experiment and theory. *Physical review letters*, 66(13):1741, 1991.

[53] Minzhong Xu and Zlatko Bačić. Inelastic neutron scattering spectra of a hydrogen molecule in a nanocavity: Methodology for quantum calculations incorporating the coupled five-dimensional translation-rotation eigenstates. *Physical Review B*, 84(19):195445, 2011.

[54] Minzhong Xu, Mónica Jiménez-Ruiz, Mark R Johnson, Stéphane Rols, Shufeng Ye, Marina Carravetta, Mark S Denning, Xuegong Lei, Zlatko Bačić, and Anthony J Horsewill. Confirming a predicted selection rule in inelastic neutron scattering spectroscopy: The quantum translator-rotator h 2 entrapped inside c 60. *Physical review letters*, 113(12):123001, 2014.

[55] Minzhong Xu, Francesco Sebastianelli, Zlatko Bačić, Ronald Lawler, and Nicholas J Turro. H 2, hd, and d 2 inside c 60: Coupled translation-rotation eigenstates of the endohedral molecules from quantum five-dimensional calculations. *The Journal of Chemical Physics*, 129(6):064313, 2008.

[56] Minzhong Xu, Francesco Sebastianelli, Zlatko Bačić, Ronald Lawler, and Nicholas J Turro. Quantum dynamics of coupled translational and rotational motions of h 2 inside c 60, 2008.

[57] Minzhong Xu, Francesco Sebastianelli, Brittney R Gibbons, Zlatko Bačić, Ronald Lawler, and Nicholas J Turro. Coupled translation-rotation eigenstates of h 2 in c 60 and c 70 on the spectroscopically optimized interaction potential: Effects of cage anisotropy on the energy level structure and assignments. *The Journal of chemical physics*, 130(22):224306, 2009.

[58] Minzhong Xu, Lorenzo Ulivi, Milva Celli, Daniele Colognesi, and Zlatko Bačić. Quantum calculation of inelastic neutron scattering spectra of a hydrogen

molecule inside a nanoscale cavity based on rigorous treatment of the coupled translation-rotation dynamics. *Physical Review B*, 83(24):241403, 2011.

[59] Minzhong Xu, Shufeng Ye, Anna Powers, Ronald Lawler, Nicholas J Turro, and Zlatko Bačić. Inelastic neutron scattering spectrum of h2@ c60 and its temperature dependence decoded using rigorous quantum calculations and a new selection rule. *The Journal of chemical physics*, 139(6):064309, 2013.

[60] CS Yannoni, RD Johnson, G Meijer, DS Bethune, and JR Salem. Carbon-13 nmr study of the c60 cluster in the solid state: molecular motion and carbon chemical shift anisotropy. *The Journal of Physical Chemistry*, 95(1):9–10, 1991.